FINAL TECHNICAL REPORT

U.S. Geological Survey
National Earthquake Hazards Reduction Program

Award Number G20AP00047

Quaternary Slip Rates and Most Recent Surface Rupture of the Bitterroot Fault, Western Montana, from Cosmogenic Radio Nuclide Dates of Offset Glacial Deposits

by

Yann Gavillot[1], Jeffrey Lonn[1] and Michael Stickney[1]

[1]Montana Bureau of Mines and Geology, Montana Technological University
1300 W. Park Street, Butte, MT 59701
Email: ygavillot@mtech.edu; Phone: (406) 496-4890

Yann Gavillot: (406) 496-4890; ygavillot@mtech.edu
Jeffrey Lonn: (406) 496-4177; jlonn@mtech.edu
Michael Stickney: (406) 496-4332; mstickney@mtech.edu

Term of Award:
April 14, 2020 – July 14, 2021

Research supported by the U.S. Geological Survey (USGS), Department of the Interior, under USGS award number G20AP00047. The views and conclusions contained in this document are those of the authors and should not be interpreted as representing the opinions or policies of the U.S. Geological Survey. Mention of trade names or commercial products does not constitute their endorsement by the U.S. Geological Survey.

ABSTRACT

The Bitterroot fault is a 100-km-long Quaternary active normal fault that bounds the eastern margin of the north-south trending Bitterroot Mountains and accommodates extension within the Intermountain Seismic Belt. Earthquake and fault history are unknown for the Bitterroot fault, although the seismic risk is potentially high given the proximity of the rapidly growing towns in the Missoula–Bitterroot valleys. New detailed mapping using LiDAR along the southern Bitterroot Range documents multiple generations of fault scarps in Holocene-Pleistocene deposits with vertical offsets that increase in magnitude with age. Fault mapping indicates a complex fault geometry characterized by an *en echelon* pattern of discontinuous segments of 45–70° east-dipping normal faults that appear to cut the older Eocene detachment fault, and locally 70–80° west-dipping antithetic normal faults. ^{10}Be cosmogenic radionuclides exposure dating technique provides *in situ* age control for 32 surface boulders (>1m) sampled in glacial deposits. Near Como Dam, two Pinedale aged glacial moraine sequences yield peak age distributions of 15.0 ± 0.4 ka and 16.4 ± 0.6 ka assuming zero erosion rate. Maximum ages on the same two Pinedale moraines yield peak ages distribution of 15.4 ± 0.4 ka and 16.8 ± 0.6 ka for 2 mm/ka erosion rate. Vertical separation of 3.5 ± 0.1 m across the dated ~16–17 ka glacial moraine offset by the Bitterroot fault scarp, yields a fault slip rate of 0.2–0.3 mm/yr. Glacial Lake Missoula high stand shorelines inset into the dated ~15 ka glacial moraine and vertically offset 4.6 ± 1.5 m by an antithetic strand of the Bitterroot fault, yield fault slip rates of 0.2–0.4 mm/yr. In the Ward Creek Fan located ~15 km to the north of Lake Como, two dated glacial debris fan sequences yield peak age distributions of 16.6 ± 0.4 ka and 62.8 ± 1.7 ka for zero erosion, and 17.0 ± 0.4 ka and 69.9 ± 2.2 ka for 2 mm/ka erosion rate. Vertical separations of 2.4 ± 0.2 m and 4.5 ± 0.1 m on the dated ~17 ka and ~63–70 ka fan surfaces offset by the Bitterroot fault, yield fault slip rates of 0.1–0.2 mm/yr and 0.1 mm/yr, respectively. Reported exposure ages are calculated using LSDn nuclide-dependent scaling age model. Our results indicate broadly consistent fault slip rates for fault segments at Lake Como (0.2–0.4 mm/yr) and Ward Creek fan (0.1–0.2 mm/yr) with an along-strike preferred average of 0.2–0.3 mm/yr for the southern Bitterroot fault. Fault scaling relations and evidence of multiple late Quaternary fault surface ruptures suggest the Bitterroot fault could produce a Mw ~7.2 earthquake. Structural model constraints and our slip rate results indicate both high angle and low angle fault geometry are possible at depth. A seismogenic low angle fault model could generate a larger earthquake of Mw > 7.2. Data from this study suggest seismic hazards from the Bitterroot fault potentially pose a significant risk to the Missoula metropolitan area, the State's second most populous region, and major infrastructures across the Missoula-Bitterroot valleys.

1. INTRODUCTION

Western Montana contains numerous Quaternary faults and is one of the most seismically active regions in the contiguous U.S. (Fig. 1), with a history of large, damaging earthquakes (1925 M6.6 Clarkston Valley, 1935 M6.3 and 6.0 Helena, 1947 M6.3 Virginia City, and 1959, M7.3 Hebgen Lake). The Missoula and Bitterroot valleys are home to over 160,000 people, representing the State's second most populous and rapidly growing regions of western Montana with vital agricultural, water, ecological, and recreational resources. Earthquake ground shaking damage to the Missoula metropolitan area alone (119, 000 people) could profoundly affect many of its communities and major infrastructures in transportation, electric transmission lines, telecommunication, and water delivery. Current hazards models as shown by the National Seismic Hazards Maps (NSHM) show a region of relatively low seismic hazards for the Missoula-Bitterroot valleys (Fig. 1b). However, the Bitterroot fault was not included in the current NSHM as these earthquake hazards assessments do not integrate results from recent studies on the Bitterroot fault (Stickney and Lonn, 2018; this study) and therefore underestimate the associated earthquake risk for the people and infrastructures in the Missoula-Bitterroot valleys.

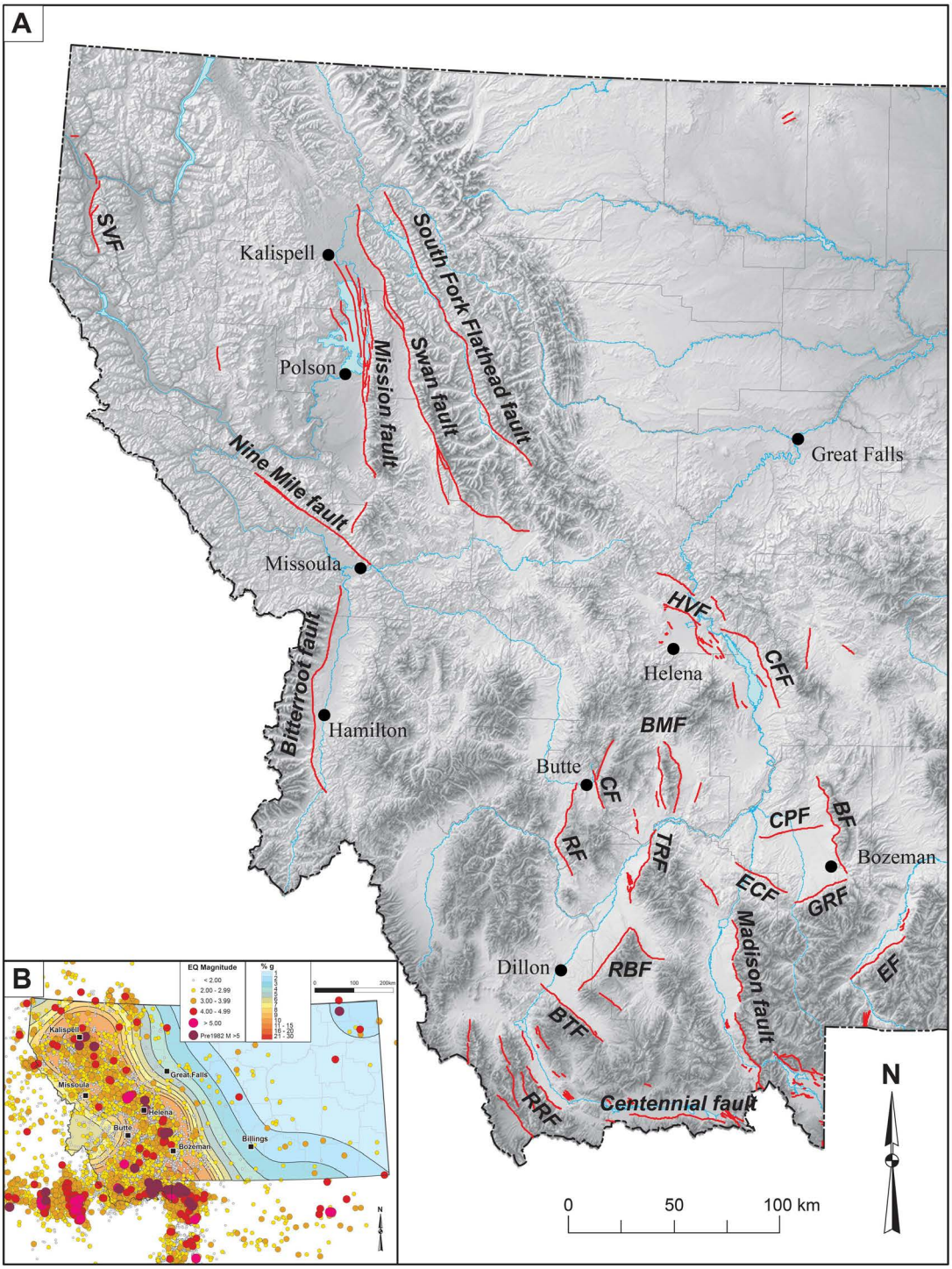

Figure 1. a) Quaternary fault database for western Montana showing names of major faults**. b)** Seismicity record between 1982-2020 from the Montana Regional Seismic Network and Montana seismic hazard map represented as peak ground acceleration with 10% probability of exceedance in 50 years. HVF: Helena Valley fault; CFF: Canyon Ferry fault; BMF: Bull Mountain fault system (Bull Mountain western border, Whitetail creek fault, Boulder River valley western border fault); CF: Continental fault; RF: Rocker fault; TRF: Tobacco Root fault; BF: Bridger fault; GRF: Gallatin Range fault; CPF: Central Park fault; ECF: Elk Creek fault; EF: Emigrant fault; RBF: Ruby Range fault system (Ruby Range northern border fault, Ruby Range western border fault); BF: Blacktail fault; RRF: Red Rock fault; SLF: Savage Lake fault.

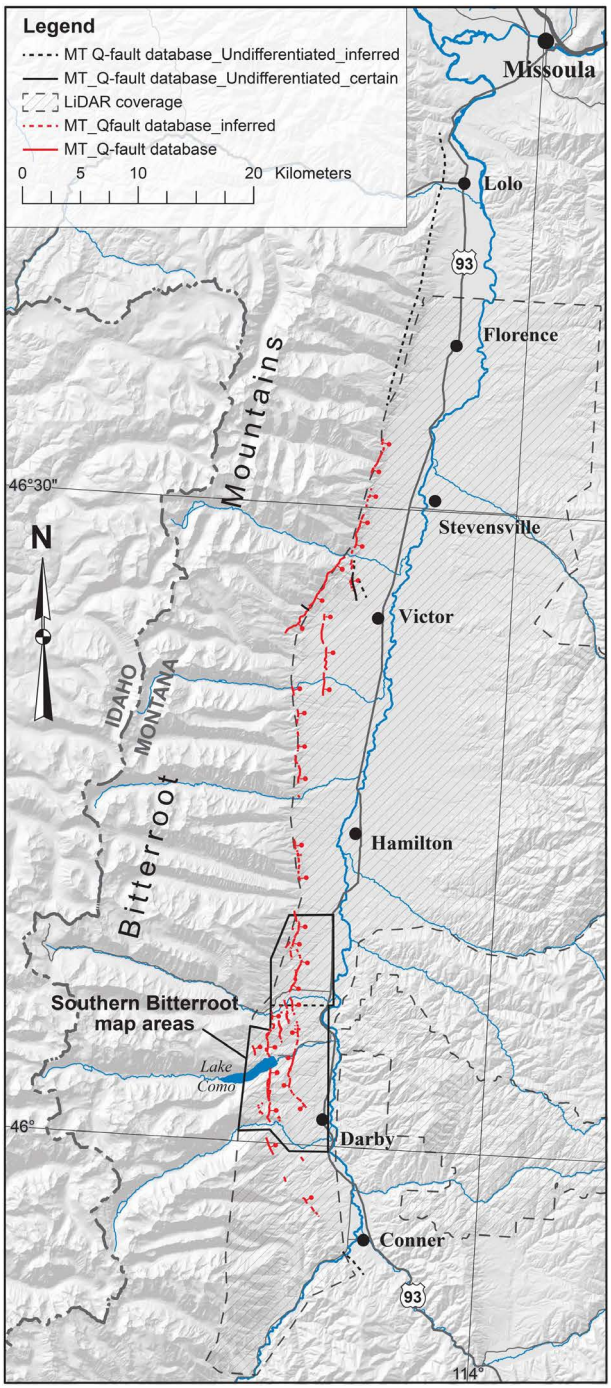

Figure 2. Quaternary fault and location map of the Bitterroot fault and Bitterroot-Missoula valleys. Base map is 10m hillshade digital elevation model (DEM). Inset box indicates location of new mapping from this study near Lake Como. Northern section of the Southern Bitterroot map areas (north of east-west dashed line) indicates revised mapping from Stickney and Lonn, 2018.

The Bitterroot fault is a 100-km-long, east-dipping normal fault that bounds the eastern margin of the north–south-trending Bitterroot Mountains (Fig. 2a). Recent LiDAR data and fault mapping by Stickney and Lonn (2018) have documented evidence of fault scarps offsetting young late Quaternary surfaces and deposits associated with the Bull Lake (>100 ka) and Pinedale glaciations (~15–20 ka) (Pierce, 2003 and references therein; Licciardi and Pierce, 2008).

Vertical offset and relative age constraints of faulted glacial deposits suggest slip rates estimates are <1 mm/yr. Earthquake history and recurrence interval are unknown for this fault, although the seismic risk is potentially high given the length of the fault, evidence of late Quaternary fault scarps, and proximity of the rapidly growing towns in the Missoula–Bitterroot valleys. Length scaling relationships suggest that a single event with a minimum of 2 m surface rupture across the entire length of the Bitterroot fault could produce a Mw ~7.2 earthquake. Larger scarps in progressively older deposits demonstrate that multiple earthquakes have occurred during the Quaternary. Scarp heights and vertical offsets of glacial, periglacial, and alluvial deposits increase in magnitude with relative age across multiple generations of fault scarps.

In this final technical report, we present new detailed mapping, using high resolution topographic data (LiDAR) with measurements of deformation, and in situ age data (CRN ^{10}Be) to define Pleistocene-early Holocene fault slip rates of the Bitterroot fault. Our new mapping and age data are located in the Southern Bitterroot map areas near Lake Como with well-preserved deformed glacial deposits, geomorphic surfaces and multiple fault scarps (Fig. 3). Improved knowledge of the fault slip rates provides new constraints on the characterization of the late Quaternary fault history and earthquake potential. Our study provides new data that constrain the along and across strike variability in fault slip partitioning and extension rates of the Bitterroot fault. Our results support ongoing efforts to update geological parameters and improve regional deformation models used in NHSM and USGS Quaternary Fault and Fold Database in the Intermountain West, as well as local

earthquake hazards assessment for the Missoula-Bitterroot valleys and its infrastructures. Moreover, this study improves our understanding of the regional tectonics of the Northern Rockies Basin and Range region.

2. GEOLOGIC SETTING

The western boundaries of the Bitterroot and Missoula valleys that include the cities of Missoula and Hamilton, are defined by the Central Bitterroot Mountains, a north–south-trending mountain range that encompasses the southernmost and tallest sub-range of the Bitterroot Mountains (Figs. 1a and 2). The Bitterroot region is located on the western margin of the Intermountain Seismic Belt (ISB), one of the most extensive zones of seismicity within the Continental U.S (Fig. 1b). The ISB is defined as a north–south-oriented 100–200 km wide zone of intraplate seismicity that extends 1,500 km from southern Nevada to northwestern Montana (Smith and Arabasz, 1991; Mason, 1996). In general, the ISB is characterized by diffuse shallow (<20 km) seismicity, Quaternary normal faults, and episodic surface-rupturing earthquakes that accommodate intra-plate extensional crustal strain within the western North American plate (Sbar, 1972; Arabasz and Smith, 1981).

The Bitterroot fault is one the longest Quaternary active faults that accommodates extension across the ISB of western Montana and Northern Rockies Basin and Range, as recognized by the recent updates to the USGS Quaternary Fault and Fold Database (e.g., Hatem et al., 2020). Fault geometry is characterized by ~100-km-long series of fault segments that mark the physiographic boundary between the eastern Bitterroot Mountains range front and the western margin of the Bitterroot Valley (Fig. 2). Fault geometry is interpreted as a steeply east-dipping normal fault that cuts the older Eocene Bitterroot detachment (B-detachment) fault inferred to extend into the subsurface of the Bitterroot Valley (Stickney and Lonn, 2018). In detail, preliminary fault mapping indicates a more complex fault geometry and fault dip characterized by *en echelon* patterns of discontinuous fault segments, including west-dipping normal faults that may accommodate part of the total slip budget as either half-graben and/or antithetic structures (Fig. 2b). The degree of slip partitioning, fault activity, and earthquake history between the different fault segments of the Bitterroot fault are unclear. Uncertainties in these parameters limit our current ability to constrain the associated seismic hazards of the Missoula–Bitterroot valleys.

Earthquake frequency and Quaternary fault activity for the Bitterroot fault are either poorly constrained or unknown when compared with other active structures across the ISB. Limited historic surface-rupturing earthquakes have occurred in southwest Montana from similar normal fault systems, such as the 1959 M7.3 Hebgen Lake earthquake (Witkind et al., 1962; Witkind 1964; Myers and Hamilton, 1964). The Hebgen Lake earthquake was one of the largest continental normal faulting events. It produced extensive multi-segment surface ruptures for >10 km with a fault scarp vertical offset of 4–6 m and a major landslide that dammed the Madison River. This event was widely felt, causing 29 fatalities, but predates the major infrastructure and population growth that has occurred in the past 60 years across western Montana.

The Bitterroot fault is likely the primary seismogenic fault system near the Missoula-Bitterroot valleys releasing interseismic strain accumulation via surface-rupturing earthquakes. Lack of significant microseismicity within the Bitterroot-Missoula valleys (Figure 1b; Stickney, 2015), may suggest the Bitterroot fault is locked at depth, and could be potentially primed for a large-magnitude, surface-rupturing earthquake. An earthquake scenario of M7.2 based on ~100 km-long surface rupture along the Bitterroot fault is forecasted to produce 'heavy' earthquake damage with .75g peak ground acceleration, 86 cm/sec peak velocity, and Modified Mercalli Intensity IX shaking (https://earthquake.usgs.gov/scenarios/catalog/mt2016/).

It is noteworthy that the Bitterroot fault is currently not included in the latest versions of the Montana seismic hazard map or USGS National Hazards Seismic Model (Fig. 1b). This omission is attributed to the lack of available slip rate and earthquake recurrence data. Limited constraints of Quaternary fault activity and lack of paleoseismic data for the Bitterroot fault emphasize the need to obtain new and improved constraints of Holocene–Pleistocene fault deformation rates and earthquake history.

No previous quantitative slip rates exist for the Bitterroot. This study provides a new dataset of numerical ages to constrain late Quaternary slip rates based on five selected offset geomorphic surfaces within three study sites, including the Lake Como, Ward Creek, and Rock Creek areas using ^{10}Be cosmogenic radionuclide dating (Fig. 3).

3. QUATERNARY MAPPING OF THE BITTERROOT FAULT

The Bitterroot fault is broadly categorized as a continuous N-S-trending normal fault with Quaternary activity that extends for ~100 km along the Bitterroot Mountains range front (Fig. 1). This fault system extends northward along the range front at least to the town of Lolo and to at least Darby on the south (Fig. 2). Recent mapping and LiDAR data (Stickney and Lonn, 2018; this study) revealed a more complex fault system along its mapped trace, characterized by along strike variability and multiple discontinuous fault segments (Figs. 2 and 3). Just north of the latitude of Victor, the northern section of the Bitterroot fault is defined as a single NNE-SSW east-dipping fault trace. Farther south, between Victor and Hamilton, the central section of Bitterroot fault consists of one, and in places to two, parallel east-dipping N-S-trending fault traces. South of Hamilton, the southern section of the Bitterroot fault consists of numerous parallel *en echelon* fault traces trending N-S to NW-SE, east- and west-dipping faults, and local fault grabens (Figs. 2 and 3).

This study produced a new, more detailed 1:24,000-scale geologic and Quaternary fault map in the Southern Bitterroot map area near Lake Como (Plate 1; Fig. 3). This map encompasses 118 km^2 and builds on previous work in the Bitterroot Valley by Lonn and Sears (2001) and Stickney and Lonn (2018).

Map relations, field observations, topographic, and cross section constraints indicate the main trace of the Bitterroot fault (BF) is an east-dipping 45–70°E normal fault (Plate 1, Figs. 3–6). East of Lake Como and the main fault trace, mapping indicates an approximately 10 km-long, 70–80° west-dipping normal fault interpreted as an antithetic structure to the main strand of the east-dipping BF (Figs. 3–6). Subsurface fault models constrained by cross section interpretation provide two permissible structural solutions for the BF as a high-angle or low angle seismogenic normal fault (Fig. 4). Fault block kinematics predict either differential deformation across the antithetic fault controlled at depth by displacement vectors of the main structure as a high angle fault (Fig. 4a); or uniform hanging wall fault-bounded block displacement due to long wavelength displacement vectors as a low angle fault (Fig. 4b). Lack of steeply sloping (>20–30°) range front facets or significant topographic gradients across the Bitterroot fault may provide supporting evidence of a low angle fault geometry (Fig. 5a). However, our mapping and cross sections indicate either fault models are possible, which have major implications for the seismogenic fault width and associated seismic hazards of Bitterroot fault (see discussion on earthquake potential).

Field observations, topographic and remote sensing analyses using LiDAR data demonstrate numerous fault scarps offset Pleistocene-Holocene deposits (Figs. 3, 5, 6; Plate 1). Fault scarps associated with the BF offsets various Quaternary surficial deposits, but local exposures indicate bedrock scarps juxtapose Eocene-Cretaceous granitic rocks in its footwall (granodiorite with mylonitic and fault breccia zones; TKg) against Quaternary deposits in its hanging wall (Plate 1; Fig. 4). Foliated bedrock that includes the Bitterroot mylonite (TKg) dips 10–43°SE, with an average of ~20°SE, is associated with the older deformation history of the Eocene Bitterroot detachment fault (referred to herein as the "B-

detachment" to avoid confusion with the Quaternary Bitterroot fault that is the focus of this study). The gently dipping B-detachment is offset and cut at the surface by the Quaternary slip along the steeply dipping Bitterroot fault (Fig. 4; Plate 1). Previous maps (Berg and Lonn, 1996; Lonn and Berg, 1996; Lonn and Sears, 2001) have shown similar map patterns along the Bitterroot range front.

Cross section interpretations indicate the deeper fault geometry of the Bitterroot fault could either remain steeply dipping or alternatively, join as a seismogenic low angle fault structural weaknesses from the preexisting ~1 km thick mylonitic fabric of the B-detachment (Fig. 4). Overlying Quaternary-Tertiary gravels (QTgc) are deposited with erosional contacts and angular unconformities on top of the B-detachment and east-tilted Eocene volcanics (Tv) exposed along the Bitterroot River (Plate 1; Fig. 4). Map relations and cross sections indicate up to ~500-600m of QTgc consistent with correlative deposits thickening northward in the Bitterroot Valley (see unit description for more details). These gravels (QTgc) are offset by Quaternary offset along the BF (Figs. 5 and 6). However cross section constraints do not suggest significant synorogenic growth associated with the BF (Fig. 4). Various glacial (Qgt, Qgo, Qdf), fluvial/alluvial (Qat, Qpa, Qaf, Qal), and landslides deposits (Qls), ranging in thickness from 1-120 m stratigraphically overlay the Quaternary-Tertiary gravels (see unit description for more details). These Quaternary units mapped across the BF demonstrate surface deformation, fault scarps, and vertical separation that increase with relative age (Plate 1, and Figs. 4–6).

4. PRE-BITTERROOT FAULT HISTORY

The core of the Bitterroot Mountains is comprised of the metamorphic infrastructure of a well-studied Eocene metamorphic core complex (e.g. Hyndman, 1980; Foster and others, 2001).

Cretaceous to Eocene intrusive rocks (TKg) mainly underlie the Bitterroot Mountains in the footwall of the 53-30 Ma B-detachment based on Apatite Fission Track (AFT) cooling ages (Foster and Raza, 2002). The gently east-dipping Eocene Bitterroot detachment (Plate 1; Fig. 4) was responsible for the rapid exhumation of these mid-crustal rocks from depths of >20 km (Foster et al, 2001). This fault exhibits a transition from amphibolite facies gneiss containing mylonitic bands to greenschist facies shearing to brittle faulting through time as structural levels became increasingly shallow.

The hanging wall of the B-detachment is comprised mainly of Mesoproterozoic metasedimentary rocks (YXm) intruded by Cretaceous to Eocene granitic rocks (TKg). Tertiary volcanic rocks (Tv) unconformably and discontinuously overlie the metamorphic-plutonic bedrock (Plate 1; Fig. 4). The age of Tv unit is unknown but inferred to be Eocene and associated with extension on the B-detachment (Berg and Lonn, 1996). In the few places where hanging wall rocks are preserved near the B-detachment along the Bitterroot range front, they are extensively brecciated, in contrast to the gneissic and mylonitized footwall rocks. The trace of the B-detachment fault is shown approximately at the contact between the amphibolite facies mylonitic gneiss, shown by mylonitic foliation/lineation symbols, and the brecciated rocks. The trace of the B-detachment is exposed discontinuously along and east of the mountain front (Plate 1).

Foster and Raza (2002) postulated that steep east-dipping normal faults in the Bitterroot Valley, including the Bitterroot fault, was Miocene in age and responsible for the uplift and exposure of the older Eocene B-detachment fault (Plate 1; Fig. 4). Stickney and Lonn (2018) postulated that erosion removed most of the brecciated and less resistant rocks of the B-detachment hanging wall, leaving the resistant gneiss of the footwall to form the planar, gently sloping Bitterroot Mountain front. However, no AFT cooling ages and exhumation younger than ~22 Ma have been recorded along the range front (Foster and Raza, 2002). A shallow sloping range front and modest topographic gradients across the Bitterroot fault (Fig. 5a), contradict a tectonically active landscape controlled by the Bitterroot fault since early Miocene.

Estimates of total fault displacement from our cross sections are consistent with the interpretation of a young (Late Miocene to Plio/Pleistocene) onset for the Bitterroot fault (Fig. 4). The Bitterroot fault may represent the modern expression of the Basin-and-Range-style extension in the Northern Rockies as a high angle normal fault (Fig. 4a). Alternatively, the Quaternary Bitterroot fault may represent a low-angle fault controlled at depth by the structural inheritance of the gentle-dipping Bitterroot detachment mylonitic gneiss (Fig. 4b).

6. LATE CENOZOIC-QUATERNARY MAP UNITS

Quaternary-Tertiary gravels

Exhumation and erosional history of the Bitterroot Mountains post-dating the B-detachment are recorded in the unconsolidated Cenozoic deposits (unit QTgc) accumulated in the Bitterroot valley to depths as great as ~700–1000m based on well-logs and gravity model constraints north of Hamilton (Norbeck, 1980; Smith, 2006; Fig. 2). Our estimates of a ~500–600m QTgc unit in the southern Bitterroot map areas are consistent with a northward thickening of correlative Cenozoic sediments and widening of the Bitterroot Valley. Fossils obtained range in age from Oligocene to Pliocene(?) (Konizeski, 1958; McMurtrey and others, 1972; Dale Hanson, Museum of the Rockies, written communication, 2018). Unit QTgc consists dominantly of sandy, well-sorted, pebble-cobble conglomerate containing rounded clasts dominantly of Belt quartzite, but also including lesser amounts of mylonitic gneiss, granite, volcanic rocks, and other metamorphic rocks. These gravels are interbedded with tuffaceous silt and clay intervals that may represent floodplain deposits. Because the clasts represent lithologies present in the entire Bitterroot River basin, Lonn and Sears (2001) interpreted QTgc as a fluvial deposit deposited by an ancestral Bitterroot River (McMurtrey and others, 1972; Lonn and Sears, 2001). Larger and more angular clasts occur near the eastern and western valley margins and appear to interfinger with and grade into the fluvial deposits; they probably represent debris-flow deposits shed from the surrounding mountains. In the map area, quartzite-dominated gravels grade upward to granite/mylonitic gneiss-dominated gravels near the top of QTgc (Fig. 5c). These granitic/gneissic clasts may be glaciofluvial and therefore Quaternary. QTgc was deposited unconformably on the underlying YXm, TKg, and Tv units that formed an irregular paleosurface with considerable relief. In most places the upper QTgc contact is an erosional pediment surface with a minimum age constrained only by the overlying Pleistocene glacial deposits. The existence of glacial till underlying the pediment surface north of Hayes Creek suggests that at least some pediment surfaces developed in the Quaternary.

Quaternary deposits

Older glacial outwash (Qgoo) and glacial debris fans (Qdfo) are eroded into and mantle the relict pediment surfaces, and are associated with older glacial till (Qgto) deposited at high levels downstream from the mouths of the Bitterroot Mountains canyons. Weber (1972) postulated that these older glacial deposits represent at least two different glacial stages. Our mapping supports his theory with three recognized lateral moraine crests within Qgto south of Lake Como (Plate 1; Fig. 7). Field observations (smooth and inflated surfaces) and topographic positions suggest these glacial moraines represent Bull Lake or older glaciation (>100 ka; Pierce, 2003, and reference therein; Liccardi and Pierce; 2008).

Younger glacial deposits (Qgom, Qgoy, Qgtm, Qgty, Qdfm, Qdfy) occur in between and topographically below incised remnants of the older glacial deposits. Fields observations of many of these young glacial moraines are characterized by hummocky surfaces and fresh boulder fields, which correlate at lower elevations to glacial outwash terraces preserved along modern stream margins. These young glacial deposits are interpreted to represent Pinedale Glaciation (~15–20 ka; Pierce, 2003 and reference therein; Liccardi and Pierce; 2008).

No *in situ* age data existed prior to this study for any of the alpine glacial deposits in the Bitterroot Mountains or western Montana. Relative age chronology and mapping of these glacial deposits are based on limited data of Pleistocene glaciation from various sites in the Rocky Mountains.

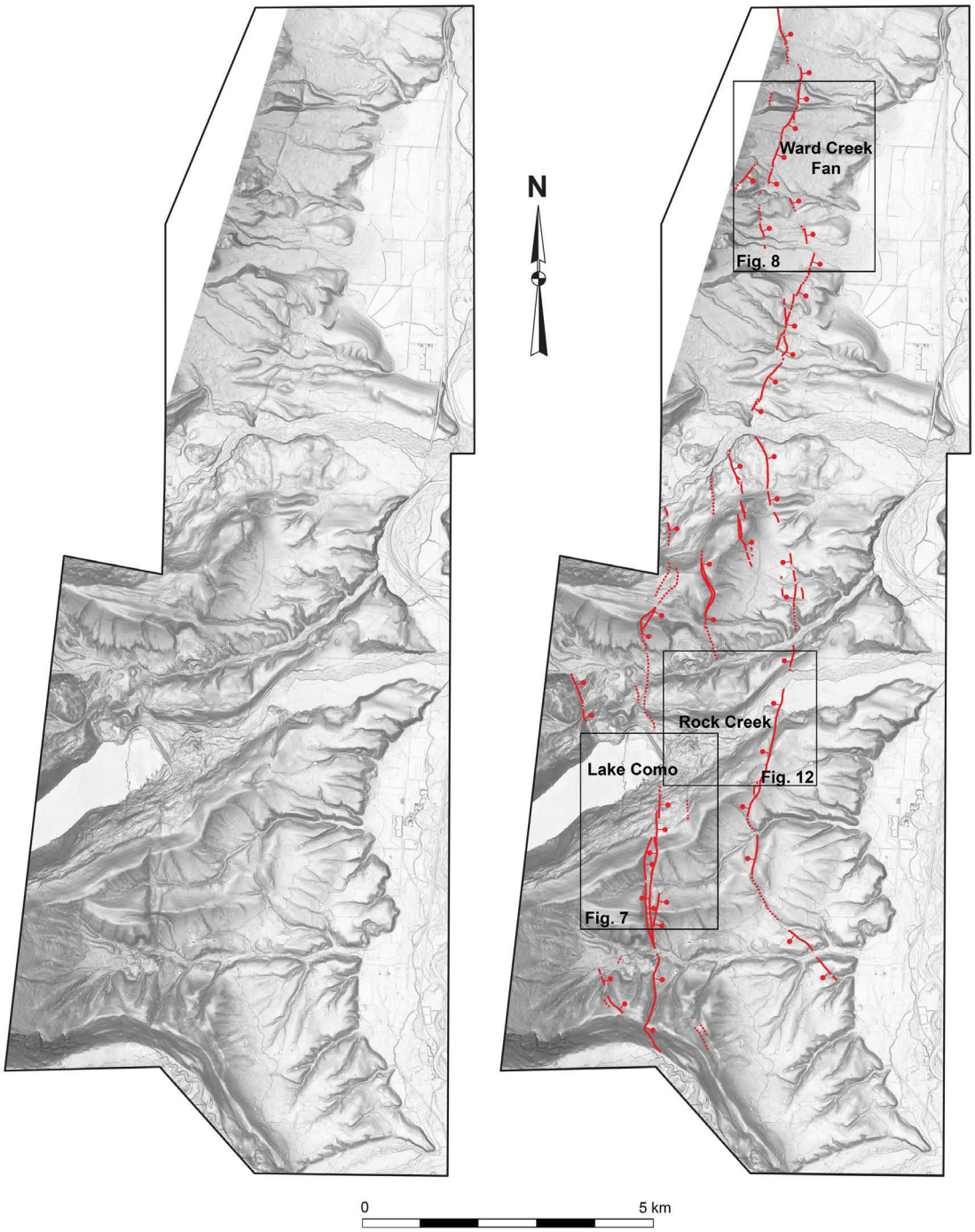

Figure 3. Quaternary fault map of the southern Bitterroot fault. See Figure 2 for location. Uninterpreted bare earth LiDAR slope shade DEM shown on the left, and map with identified fault scarps shown on the right. Inset boxes are study sites showing detailed offset geomorphic surfaces and cosmogenic ^{10}Be ages at Lake Como (Fig. 6), Ward Creek Fan (Fig. 7), and Rock Creek study sites (Fig. 12).

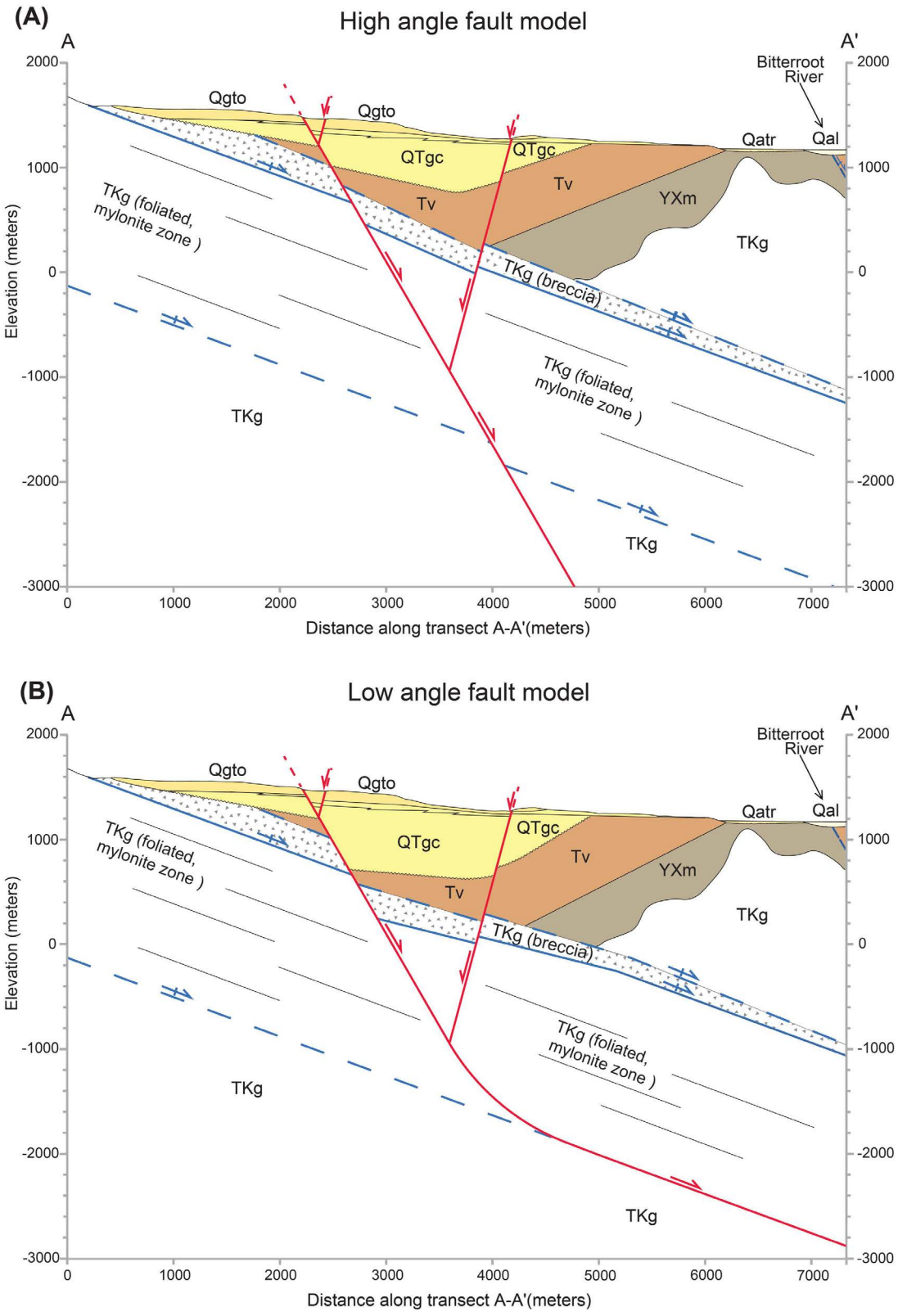

Figure 4. Structural cross sections of the Bitterroot fault showing two viable subsurface fault models that restore to the same pre-Bitterroot fault geometry: **a)** High angle fault model; **b)** Low angle fault model. See Plate 1 for transect A-A' location.

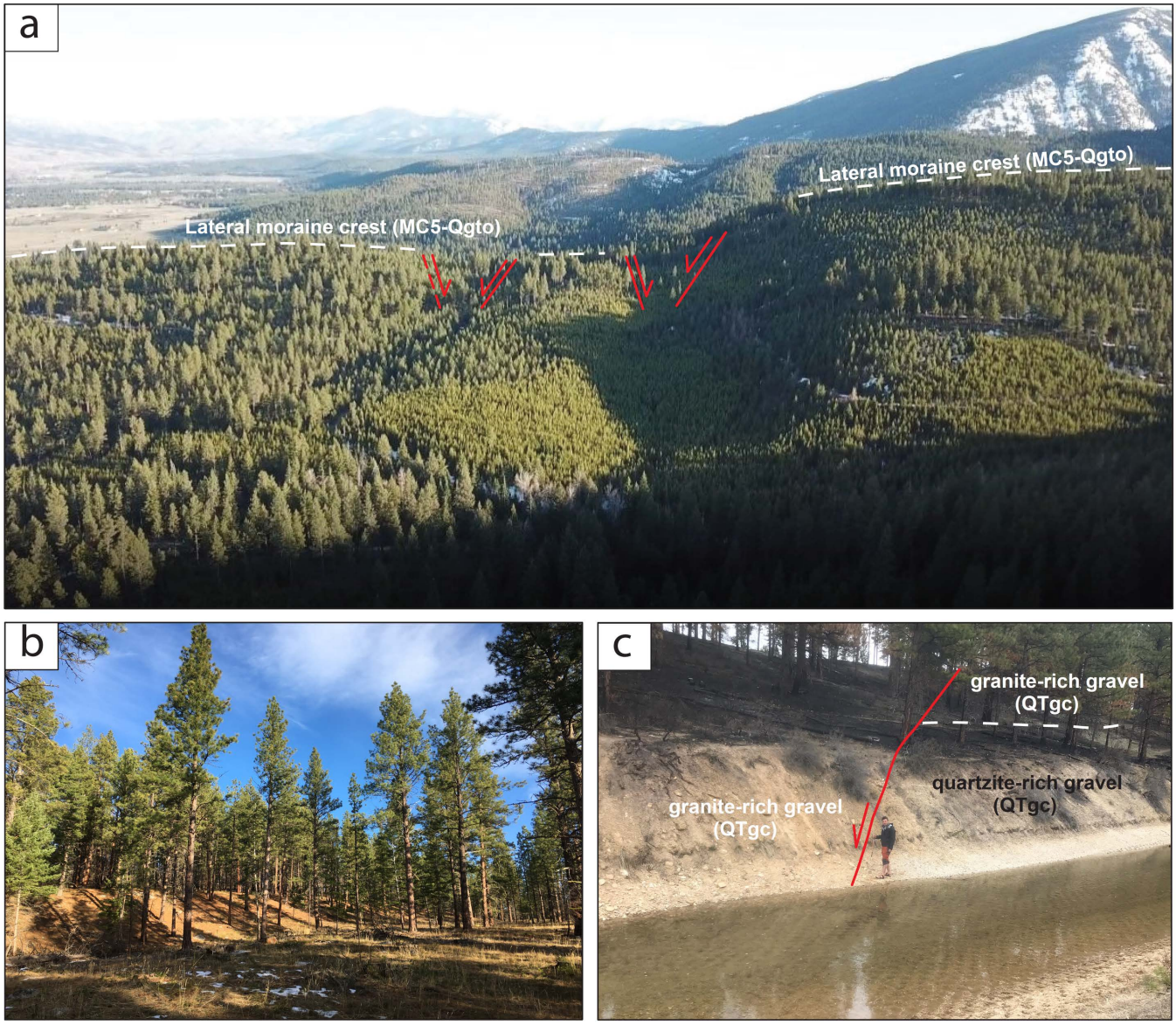

Figure 5. Field photos of Bitterroot fault scarps. a) View to the south showing in the background gentle (~20–30°) east sloping range front of the Bitterroot Mountains controlled by the B-detachment mylonite, and in the foreground the high angle fault scarps that offset old glacial moraine deposits (Qgto) with a fault scarp height of ~75 m. b) View to the NW of well exposed ~10m-high fault scarp offsetting S2 (Qdfm), a middle-aged (>Pinedale) glacial debris fan surface at the Ward Creek Fan. c) View to the NE of an outcrop exposure of the west-dipping antithetic fault near Rock Creek truncating deposits within the Quaternary-Tertiary gravels (QTgc).

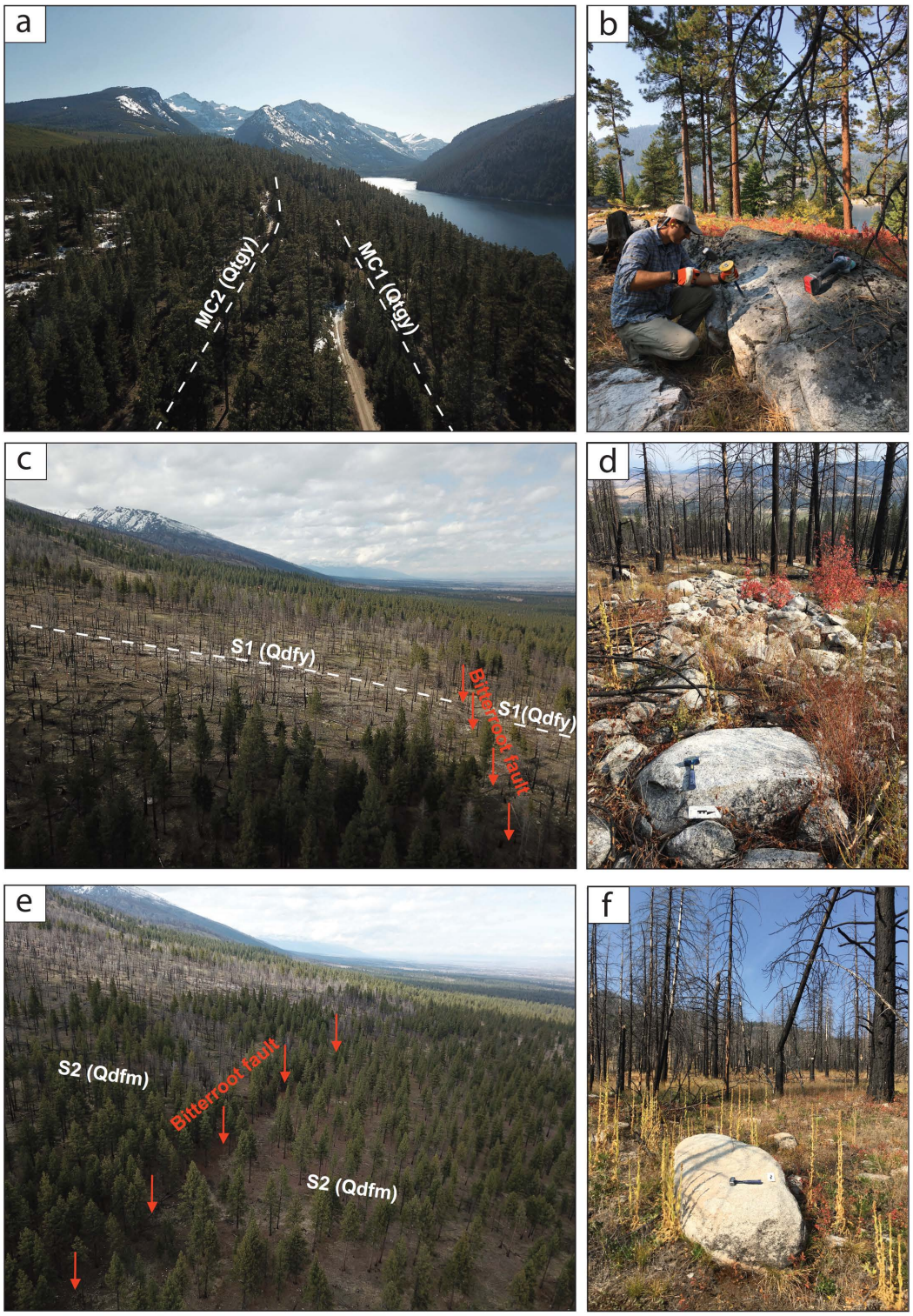

Figure 6. Field photos of geomorphic surfaces with boulders sampled for cosmogenic ^{10}Be dating. **a)** View to the west showing the young Pinedale age glacial lateral moraines (MC1–MC2) sourced from Rock Creek Glacier. **b)** Example of boulder sampled for age dating along moraine crest near Lake Como. **c&e)** Views to the north showing the young (S1) and middle-aged (S2) glacial debris fans at the Ward Creek Fan site offset by the Bitterroot fault. **d&e)** Examples debris flows surface morphology and boulder fields sampled for age dating on surface S1**(d)** and S2 **(e)**.

7. QUATERNARY GEOCHRONOLOGY

Methods

We employed cosmogenic radionuclide (CRN) methods to date geomorphic surfaces for age exposures on glacial moraines at the Lake Como study sites (Fig. 7) and glacial debris fans at the Ward Creek study sites (Fig. 8).

Surface exposure dating is establish using ^{10}Be isotopes from the quartz-rich bedrock or sediments (e.g., Gosse and Phillips, 2001; Frankel et al., 2007; Hidy et al., 2010). Sampling strategy targeted surface boulders >1 m in diameter sourced from the Eocene-Cretaceous foliated granodiorite and mylonite bedrock (TKg) and consisted of collecting the uppermost cm of the boulder surface with a battery-power angle gridder with diamond blade, hand chisel, and hammer (Fig. 6). Each sampling interval was confined to a 1 ± 0.5 cm thick sampling horizon. A minimum of 5–6 boulders were sampled for each geomorphic surface that have topographic profiles ranging from 250–750 m perpendicular to the fault scarps. Sampling selection avoided boulders that display potential evidence of post-exposure modification (spallation, uneven weathering, lack of glacial abrasion surfaces, tree uprooting, soil deflation, anthropogenic activity) or inheritance from previous surface exposure history (irregular shape, very large >3 m size boulders, dichotomy of boulder surface appearance).

Samples were processed for physical separation at the Montana Bureau of Mines and Geology (MBMG), and then sent to the Center for Accelerator Mass Spectrometry (CAMS), Lawrence Livermore National Lab (LLNL) for the Beryllium and AMS lab analytical results processed by Alan Hidy. Beryllium (Be) from the quartz fraction separated from each amalgamated boulder surface rock chips following similar methods given in Kohl and Nishiizumi (1992) and Licciardi (2000). An accelerator mass spectrometer measured the ^{10}Be isotopic concentrations. Following Be extraction procedures and isotopic concentrations measurements, CRONUS Age Calculator from Balco et al., (2008) provided the age models for each surface exposure age sample. This approach yielded surface ages that account for post-depositional exposure and erosion (Table 1; Supplemental File). Age models include measured density constraints of sampled boulders deposits of 2.6 ± 0.1 g/cm^3 for bedrock foliated granodiorite and mylonite boulders. Local site production rates for each surface sample are determined using revised spallogenic and muonogenic production rate calibrations of Heyman (2014) in the CRONUS online calculator (Balco et al., 2008), scaled for topographic shielding, latitude, and elevation using the constant production-rate models of Lal (1991) and Stone (2000). Age results and uncertainties for each boulder are reported at the 1 sigma level using the nuclide-depended scaling age model by Lofton-Stato-Dunai and assume zero erosion rate. However, because erosion rates are unconstrained for our study sites, we also provide maximum ages using long-term erosion rates of 2 mm/ka (Table 1), consistent with resistant granite-type bedrock lithology supported by analytical studies (Jackson et al., 1997; Duxbury et al., 2015, Margold et al., 2019). Modelled ages for each geomorphic surface combine multiple age results based on 5 to 11 boulders using the Density Plotter of Vermeesh et al (2012), which integrates the range of erosion rate of e=0 and e=2 mm/ka, as minimum and maximum ages, respectively. Detailed sample information, AMS results, and age model parameters for CRN ^{10}Be geochronology are provided in Table 1 and Supplementary File 1.

TABLE 1. Comosgenic 10Be sample data and modeled surface exposure ages.

Sample	Lat	Long	Elv (m)	Sample thickness (cm)[a]	Quartz mass (g)[b]	Shield Correction[c]	$^{10}Be/^{9}Be$ ($x10^{-15}$)[d]	^{10}Be concentration ($x10^{3}$ atoms/g SiO_2)[d]	Age (zero erosion; ka)[e,f]	Age (2 mm/ka erosion; ka)[e,f]
Lake Como Morraine:										
MC1 (Qgty)										
LCS-Qgty-MC1-upper-1	46.057183	-114.236761	1355	1	21.70	0.989542	290.97 ± 5.86	208.66 ± 4.49	15.2 ± 1.0	15.5 ± 1.0
LCS-Qgty-MC1-upper-2	46.057924	-114.234597	1345	1	12.61	0.998349	156.47 ± 2.91	192.41 ± 3.86	14.0 ± 0.9	14.3 ± 0.9
LCS-Qgty-MC1-lower-3	46.058918	-114.232156	1329	1	25.07	0.998845	343.67 ± 6.80	215.21 ± 4.55	15.8 ± 1.0	16.2 ± 1.0
LCS-Qgty-MC1-lower-4	46.05983	-114.23092	1327	1	25.02	0.998562	335.23 ± 6.23	209.06 ± 4.19	15.4 ± 1.0	15.8 ± 1.0
LCS-Qgty-MC1-fault-5	46.058095	-114.234252	1346	1	25.00	0.998455	326.05 ± 6.05	204.68 ± 4.10	14.9 ± 0.9	15.2 ± 1.0
Lake Como Morraine:										
MC2 (Qgty)										
LCS-Qgty-MC2-lower-1	46.056855	-114.233578	1366	1	24.99	0.997926	361.68 ± 7.66	225.40 ± 5.06	16.1 ± 1.0	16.5 ± 1.1
LCS-Qgty-MC2-lower-2	46.056771	-114.233924	1367	1	9.86	0.998534	122.24 ± 2.27	191.78 ± 3.85	13.7 ± 0.9	14.1 ± 0.9
LCS-Qgty-MC2-lower-3	46.056698	-114.234311	1373	1	24.99	0.996904	358.30 ± 6.23	224.21 ± 4.24	15.9 ± 1.0	16.3 ± 1.0
LCS-Qgty-MC2-upper-4	46.056456	-114.234938	1380	1	25.10	0.998948	369.92 ± 7.08	231.45 ± 4.75	16.2 ± 1.0	16.6 ± 1.1
LCS-Qgty-MC2-upper-5	46.05633	-114.235173	1387	1	25.03	0.998404	475.66 ± 9.09	297.54 ± 6.10	20.6 ± 1.3	21.2 ± 1.4
LCS-Qgty-MC2-upper-6	46.055926	-114.235900	1395	1	25.01	0.997285	410.52 ± 6.74	254.25 ± 4.58	17.6 ± 1.1	18.1 ± 1.2
Ward Creek Fan:										
S1-Lower (Qdfy)										
WCF-Qdfy-S1-lower-1	46.16152	-114.215608	1321	1	19.98	0.996478	426.38 ± 7.70	331.02 ± 6.47	23.9 ± 1.5	24.8 ± 1.6
WCF-Qdfy-S1-lower-2	46.161483	-114.215093	1315	1	20.01	0.996817	275.98 ± 5.15	219.44 ± 4.42	16.2 ± 1.0	16.6 ± 1.1
WCF-Qdfy-S1-lower-3	46.161692	-114.214868	1315	1	20.03	0.996804	873.31 ± 10.77	691.31 ± 9.96	50.0 ± 3.1	54.9 ± 3.7
WCF-Qdfy-S1-lower-4	46.161944	-114.215443	1323	1	20.01	0.959965	345.08 ± 5.43	274.34 ± 4.78	20.8 ± 1.3	21.4 ± 1.4
WCF-Qdfy-S1-lower-5	46.162041	-114.215004	1317	1	20.02	0.99636	372.66 ± 6.02	297.06 ± 5.29	21.8 ± 1.4	22.5 ± 1.4
WCF-Qdfy-S1-lower-6	46.162061	-114.215653	1325	1	20.01	0.996981	287.76 ± 5.37	229.40 ± 4.62	16.9 ± 1.1	17.4 ± 1.1
Ward Creek Fan:										
S1-Upper (Qdfy)										
WCF-Qdfy-S1-upper-1	46.162111	-114.216519	1335	1	20.09	0.99496	291.22 ± 5.45	229.49 ± 4.62	16.9 ± 1.1	17.3 ± 1.1
WCF-Qdfy-S1-upper-2	46.161994	-114.217598	1348	1	20.00	0.996759	306.94 ± 5.71	245.26 ± 4.91	17.6 ± 1.1	18.1 ± 1.2
WCF-Qdfy-S1-upper-3	46.161917	-114.2182	1355	1	20.24	0.995886	284.58 ± 6.48	224.17 ± 5.37	16.1 ± 1.0	16.5 ± 1.1
WCF-Qdfy-S1-upper-4	46.161944	-114.218611	1360	1	20.02	0.996257	282.49 ± 5.72	225.06 ± 4.86	16.1 ± 1.0	16.5 ± 1.1
WCF-Qdfy-S1-upper-5	46.161755	-114.216547	1334	1	20.01	0.99278	221.9 ± 4.12	176.26 ± 3.53	13.0 ± 0.8	13.3 ± 0.8
Ward Creek Fan:										
S2-Lower (Qdfm)										
WCF-Qdfm-S2-lower-1	46.158698	-114.216225	1310	1	25.00	0.996981	2395.16 ± 36.64	1307.93 ± 22.26	95.7 ± 6.0	113.8 ± 8.6
WCF-Qdfm-S2-lower-2	46.158274	-114.21334	1280	1	25.00	0.996981	2066.43 ± 32.69	1282.49 ± 22.42	96.2 ± 6.0	114.4 ± 8.7
WCF-Qdfm-S2-lower-3	46.158213	-114.211642	1267	1	25.02	0.996968	1517.05 ± 20.34	944.80 ± 14.49	71.6 ± 4.4	81.5 ± 5.8
WCF-Qdfm-S2-lower-4	46.156498	-114.216332	1289	1	25.00	0.996969	1485.56 ± 18.05	836.78 ± 11.93	62.5 ± 3.9	69.5 ± 4.8
WCF-Qdfm-S2-lower-5	46.157164	-114.214925	1285	1	25.04	0.996981	2221.56 ± 26.88	1381.75 ± 19.63	103.1 ± 6.4	124.7 ± 9.6
Ward Creek Fan:										
S2-Upper (Qdfm)										
WCF-Qdfm-S2-upper-1	46.159341	-114.21877	1344	1	25.02	0.996977	1264.89 ± 15.09	790.83 ± 11.12	56.4 ± 3.5	62 ± 4.2
WCF-Qdfm-S2-upper-2	46.160737	-114.220153	1373	1	25.03	0.996758	1553.44 ± 26.51	966.22 ± 17.99	66.9 ± 4.2	75.4 ± 5.4
WCF-Qdfm-S2-upper-3	46.160691	-114.221614	1384	1	25.00	0.996127	466.97 ± 7.90	291.70 ± 5.40	20.2 ± 1.3	20.9 ± 1.3
WCF-Qdfm-S2-upper-4	46.160441	-114.220668	1374	1	25.01	0.996981	1336.26 ± 20.58	832.02 ± 14.23	58.0 ± 3.6	63.9 ± 4.4
WCF-Qdfm-S2-upper-5	46.159012	-114.217954	1333	1	25.01	0.994069	2113.33 ± 24.92	1313.49 ± 18.32	94.7 ± 5.9	112.3 ± 8.5

[a] Sample thickness represents the total amount of material modelled for ^{10}Be exposure dating that includes 1.0 ± 0.5 cm of bedrock (granodiorite-gneiss) sampled interval.

[b] Average measured density of foliated biotite-muscovite granodiorite to gneiss boulder samples (2.57 ± 0.1 g/cm^3).

[c] Geometric shielding correction using CRONUS online calculator

[d] All uncertainties reported at the 1-sigma level.

[e] Ages reported using LSDn (Nuclide-dependent scaling age models by Lifton-Stato-Dunai)

[f] Assumed value of erosion rates for stable and resistant foliated granodiorite boulders that have preserved glacial erosional surfaces.

Age results generated by CRONUS-Earth online calculators, Balco et al. (2008).
https://hess.ess.washington.edu/
version 3

Ages of Pinedale glacial moraines – Lake Como

MC1(Qgty)

The youngest glacial till deposits sampled for CRN ^{10}Be dating were collected on surface boulders along a lateral moraine crest, referred as MC1, in the Lake Como study site (Figs. 6a–b and 7). The sampled surface MC1 represents the lowest and best-preserved moraine crest mapped south of Lake Como within the young glacial deposits (*Qgty*; Plate 1), sourced from the Pinedale age Rock Creek Glacier and extends nearly perpendicularly across the Bitterroot fault (Fig. 7). A total of 5 boulders were sampled along a 500 m length of the ENE-WSW-trending moraine crest, yielding ages from lowest to highest elevations (1327–1355 m) of 15.4 ± 1.0 ka, 15.8 ± 1.0 ka, 14.0 ± 0.9 ka, 14.9 ± 0.9 ka, and 15.2 ± 1.0 ka (Fig. 7; Table 1). Model age results and probability density plots combining all boulders from MC1 yield peak ages that range between 15.0 ± 0.4 ka and 15.4 ± 0.4 ka for erosion rates of e=0 and e=2 mm/ka, respectively (Fig. 9). The model age of ~15 ka for MC1 indicate no significant age difference between boulder ages results that account for erosion rates. This sensitivity analysis suggests that potential erosion does not affect our age results.

MC2 (Qgty)

Another young glacial till deposit (*Qgty*) south of Lake Como was sampled on surface MC2, an ENE-WSW-trending lateral moraine crest that occupies a higher elevation than MC1 (Figs. 6a and 7; Plate 1). A total of 6 boulders were sampled along a 250m-long profile of MC2 offset by the Bitterroot fault scarp (Fig. 7). Boulder sample population yield ages from lowest to highest elevation (1366-1395 m) of 16.1 ± 1.0 ka, 13.7 ± 0.9 ka, and 15.9 ± 1.0 ka, 16.2 ± 1.0 ka, 20.6 ± 1.3 ka, and 17.6 ± 1.1 ka (Fig. 7; Table 1). Model age results of MC2 combining all boulders yield peak ages that range between 16.4 ± 0.6 ka (e=0) and 16.8 ± 0.6 ka (e = 2 mm/ka) (Fig. 9). The model age of ~16–17 ka for MC2 indicates no significant age sensitivity with the range of erosion rates. The ~20.6 ka and ~13.7 ka boulder ages are identified as statistical outliers.

Ages of glacial debris fans – Ward Creek Fan

S1 (Qdfy)

A young glacial debris fan deposit, referred as S1, was sampled for CRN ^{10}Be dating in the Ward Creek Fan study site north of Lake Como (Figs. 6c-d and 8; Plate 1). The sampled surface S1 represents the youngest mapped debris flows and fan surface (*Qdfy;* Plate 1) within the Ward Creek Fan complex sourced from the Ward Cirque Glacier. Surface S1 is distinguished as the youngest surface with well-preserved debris flow levees incised into older surfaces (S3–S4) and extensive boulder fields (Fig. 6d and 8). S1 slopes to the east and is offset across the Bitterroot fault scarp with correlative hanging wall and footwall surfaces (Fig. 6c and 8). Across ~300 m-long profile, a total of 11 boulders were sampled. The 6 boulders sampled in the lower hanging wall fan surface (S1-Lower) yield ages of 23.9 ± 1.5 ka, 16.2 ± 1.0 ka, 50.0 ± 3.1 ka, 20.8 ± 1.3 ka, 21.8 ± 1.4 ka, 16.9 ± 1.1 ka. (Fig. 8; Table 1). The 5 boulders sampled in the upper footwall surface (S1-Upper) yield ages of 16.9 ± 1.1 ka, 17.6 ± 1.1 ka, 16.1 ± 1.0 ka, 16.1 ± 1.0 ka, 13.0 ± 0.8 ka (Fig. 8; Table 1). Model age results for S1 combing all boulders across both correlative surfaces yield peak ages that range between 16.6 ± 0.4 ka (e=0) and 17.0 ± 0.5 ka (e = 2 mm/ka) (Fig. 9). The model age of ~16–17 ka for S1 indicates no significant age sensitivity with the range of erosion rates. Two of the eleven boulder age results from both lower and upper surfaces are identified as outliers, interpreted to represent inheritance from older exposure history (~50 ka) and post-exposure modification soil deflation due to footwall head scarp diffusion (~13 ka).

S2 (Qdfm)

Fan surface S2 is an older middle-aged glacial debris flow and fan deposits *(Qdfm),* mapped within the Ward Creek Fan complex sampled for CRN ^{10}Be dating (Fig. 6e-f and 8; Plate 1). Surface S2 represents the most extensive east-sloping fan surface offset by the Bitterroot fault. S2 is distinguished as a broad surface with sparse boulder fields incised by S1 and topographic lower than older surfaces S3–S4 (Figs. 6e-f, and 8). A total of 10 boulders were collected along a ~750 m-long profile across both correlative lower hanging wall and upper footwall surfaces (Figs. 6e and 8). Lower surface samples (S2-Lower) from 5 boulders yield ages of 95.7 ± 6.0 ka, 96.2 ± 6.0 ka, 71.6 ± 4.4 ka, 62.5 ± 3.9 ka, and 103.1 ± 6.4 ka (Fig. 8; Table 1). Upper surface samples (S2-Upper) from 5 boulders yield ages 56.4 ± 3.5 ka, 66.9 ± 4.2 ka, 20.2 ± 1.3 ka, 58.0 ± 3.6 ka, and 94.7 ± 5.9 ka (Fig. 8; Table 1). Model age results for S2 across both correlative surfaces yield two peak ages. The youngest model peak has ages that range between 62.8 ± 1.7 ka (e=0) and 69.9 ± 2.2 ka (e = 2 mm/ka) that we interpret as the representative exposure age for S2 (except for an outlier of ~20 ka; Fig. 9). The older peak ages (~97–116 ka; Fig. 9) are attributed to represent either inheritance or an older sequence of debris flows that were not fully buried by thin boulder veneers of the younger debris flows (~63–70 ka). In addition, S2 topographic position coincides with mapped elevations of the Glacial Lake Missoula high stand shorelines (Fig. 8; Plate 1), which may have eroded and partly exposed older debris flow deposits to the surface. Values of erosion rates effect our model age for S2 by 10% between its minimum (~63 ka) and maximum (~70ka), which may represent a larger degree of uncertainty for our age model interpretation on this surface dated with CRN ^{10}Be.

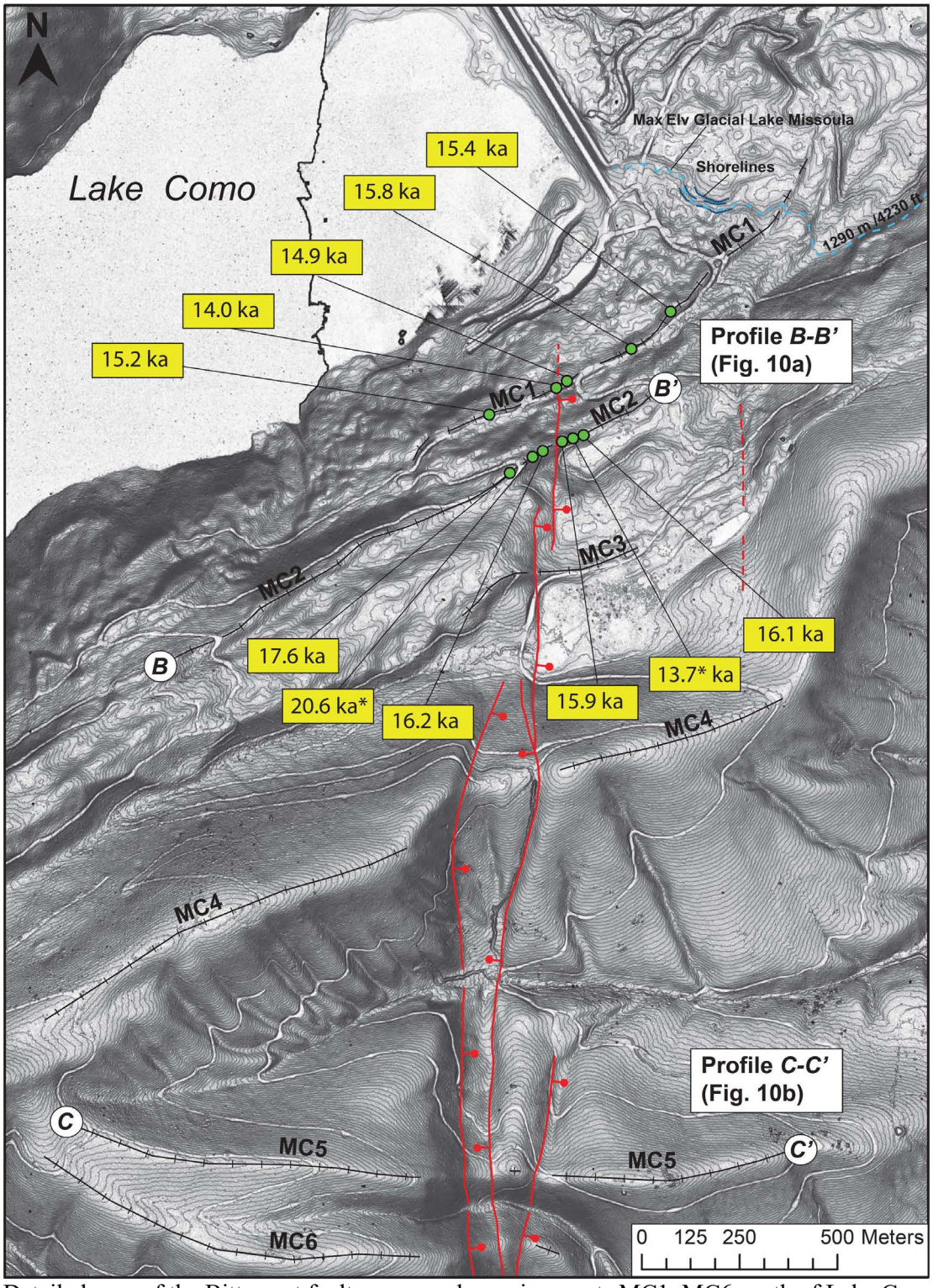

Figure 7. Detailed map of the Bitterroot fault scarps and moraine crests MC1–MC6 south of Lake Como showing cosmogenic ^{10}Be ages results from sampled boulders. Base map is LiDAR slope hillshade DEM with 2 m contour interval. See Figure 4 for location and Table 1 for age results. MC1–MC2: Young Pinedale moraine crests in glacial till (Qgty); MC3: Middle-aged moraine crest in glacial till (Qgtm); MC4–MC6: Old Bull Lake (?) moraine crests in glacial till (Qgto). *Ages identified as outliers based on probability density plots age models (Fig. 9).

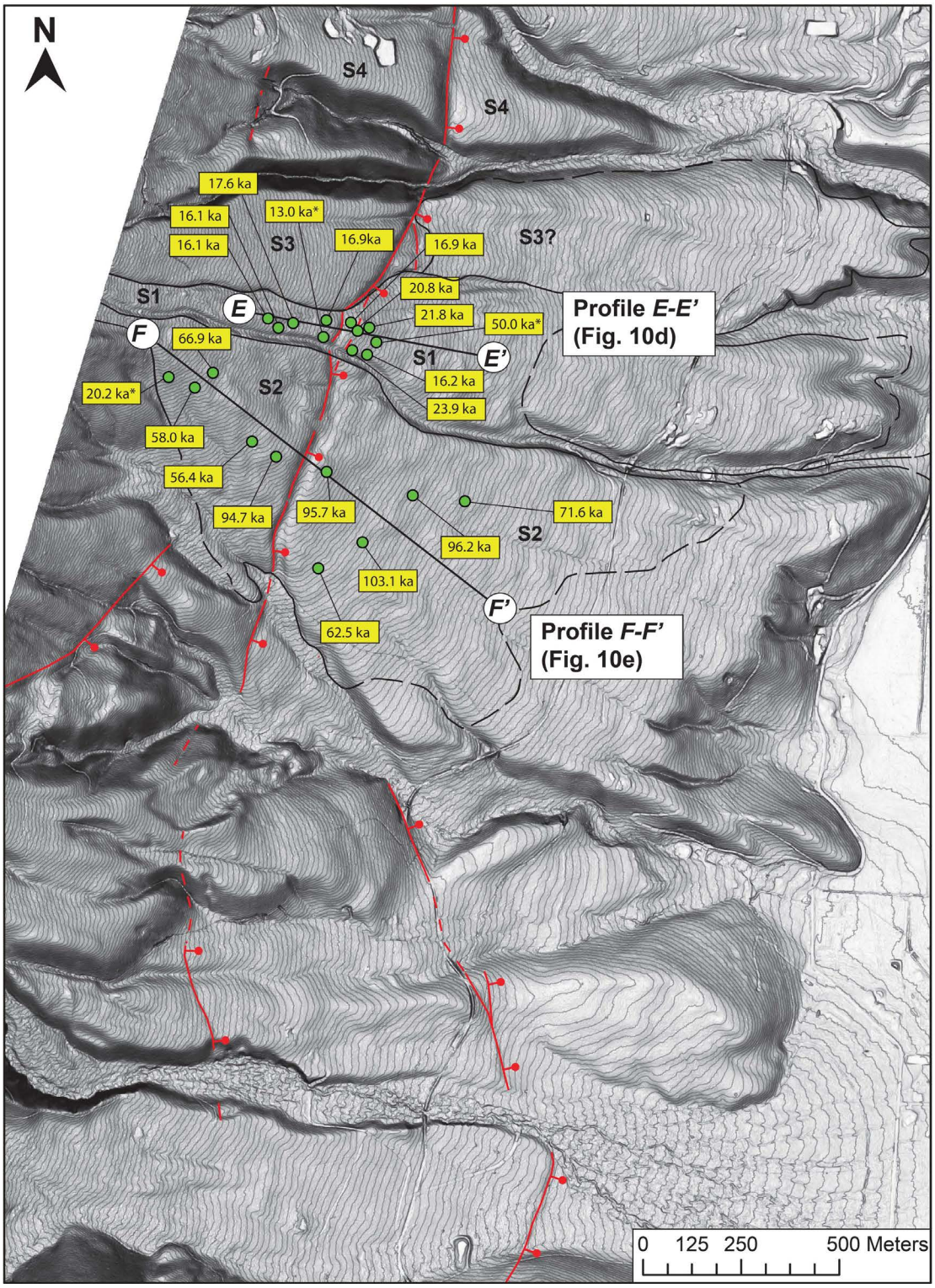

Figure 8. Detailed map of the Bitterroot fault scarps and surfaces S1–S4 at the Ward Creek Fan showing cosmogenic ^{10}Be ages from sampled boulders. Base map is LiDAR slope hillshade DEM with 2 m contour interval. See Figure 4 for location and Table 1 for age data results. S1: Pinedale young glacial debris fan (Qdfy); S2: Middle-aged glacial debris fan (Qdfm); S3: Middle-aged glacial debris fan (Qdfm) with bedrock pediment exposures. S4: Bedrock pediment surface with thin or no deposits preserved. *Ages interpreted as outliers based on probability density plots age models (Fig. 9).

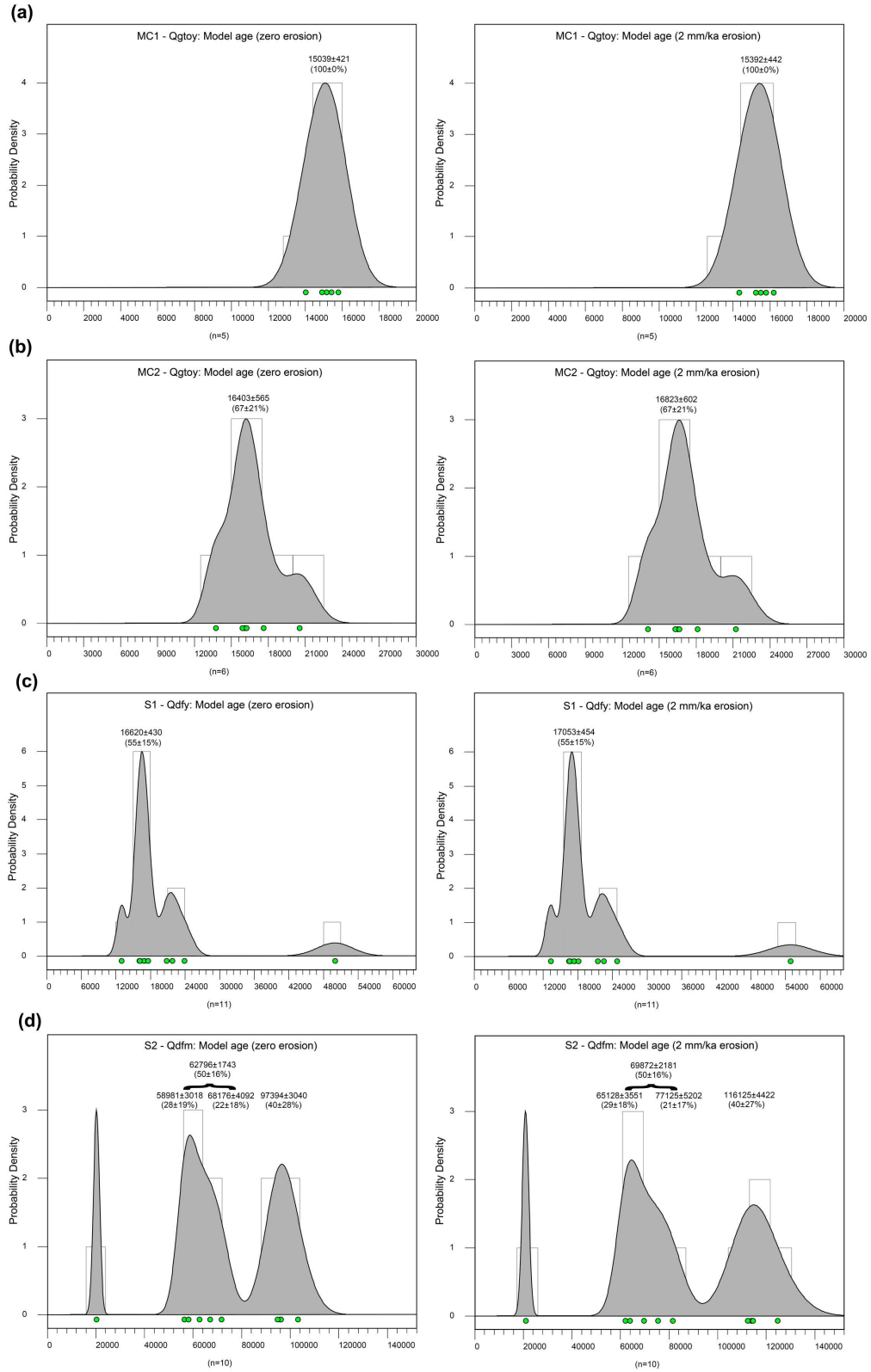

Figure 9. Probability density and histograms plots for each geomorphic unit with corresponding age model results for zero erosion (left) and 2mm/ka erosion (right). **a-b)** MC1–MC2 (Qgty): Young Pinedale age moraine crests in glacial till at Lake Como. **c)** S1 (Qdfy): Young Pinedale age glacial debris fan at Ward Creek Fan. D) S2 (Qdfm): Middle-aged glacial debris fan at Ward Creek Fan.

Age summary

Our CRN ^{10}Be age data provide a *in situ* chronology of surface exposure ages consistent with map relations of Quaternary units. In Lake Como, CRN ^{10}Be age data from two sequences of the youngest and best-preserved Pinedale glacial moraines MC1 and MC2, yield ages of ~15 ka and 16–17 ka, respectively (Fig. 7 and 9a–b; Table 1). Older mapped glacial moraines sourced from Rock Creek Glacier are consistent with our ages results, indicating MC3 as likely early Pinedale in age (>20 ka), and MC4–MC6 ka as likely Bull Lake and older in age (>100 ka). In Ward Creek Fan, age data from two glacial debris fans S1 and S2, yield ages of 16–17 ka and 63–70 ka, respectively (Fig. 8 and 9c–d; Table 1).

Our study sites in both Lake Como glacial moraines and debris fans sourced from the Ward Cirque Glacier indicate similar Pinedale age results between 15–17 ka, consistent with Pinedale ages reported in Greater Yellowstone and Teton range (15–19 ka; Liccardi and Pierce; 2008). The glacial debris fan surface (S2) of 63–70 ka at the Ward Creek Fan may correlate to MIS 4 or Early Wisconsin Glaciation (~60–70 ka), while the older boulder age population in S2 of 97–116 ka may represent exposure inheritance from MIS 6 or Bull Lake Glaciation (>100 ka) (Pierce, 2003 and references therein; Liccardi and Pierce; 2008).

8. FAULT OFFSET AND SLIP RATES

The Bitterroot fault offsets various geomorphic surfaces with scarp heights that range from 1–100 m that increase with age. Bull Lake and older glacial moraines and pediment surfaces exhibit the largest scarps, followed by younger Pinedale glacial moraines, glacial debris fans, and outwash surfaces. This study provides corresponding in-situ age data for these glacially sourced deposits at the Lake Como and Ward Creek study sites (Figs. 7–8; Plate 1).

Fault scarps truncate multiple sequences of sloping lateral moraine crests or glacial debris fans that provide geomorphic strain markers to measure vertical separation using LiDAR-based topographic profiles (Figs 7, 8, 10). Offset measurements are based on vertical separations of regression slope profiles between footwall and hanging surfaces projected across the fault scarp (Fig. 10). To determine deformation rates, we divide the amount of vertical separation, extension, and fault slip by our age data (Table 2). Fault dip and structural model constraints from map relations allow for the vertical component of deformation to be translated into fault slip rates. Fault slip rates are provided as a range with minimum and maximum values. All rates incorporate uncertainties in fault dip, age, and vertical separation for offset markers.

Lake Como

Pinedale glacial moraines: MC1–MC2 (Qgty)

South of Lake Como, the trace of the Bitterroot fault offsets young Pinedale-aged glacial till deposits (Qgty*)* and its lateral moraines MC1–MC2 (Fig. 7). Mapping and LiDAR data indicate no clear fault scarps across moraine crest MC1 (Fig. 7). A well-exposed N-S-trending east-dipping fault scarp lineament and ENE-WSW-sloping MC2 provide geomorphic strain markers of vertical separation (Figs. 7 and 10a). Topographic profile measurements yield a vertical separation of 3.5 ± 0.1 m for correlative offset surfaces across the fault scarp (Fig. 10a; profile B-B'). Map and topographic relations of the main trace of the Bitterroot fault south of Lake Como indicate the fault dips 55–70° to the East (Figs. 4 and 7). Rate calculations using an age range of 16.6 ± 0.4 ka and 17.1 ± 0.5 ka for MC2 yield a fault slip rate of 0.21–0.28 mm/yr (Table 2).

Bull Lake glacial moraines: MC4–MC6 (Qgto)

The trace of the Bitterroot fault offsets older glacial till deposits (Qgto) with three mapped

moraine crests (MC4–MC6) interpreted as Bull Lake age or older. Mapping and field observations based on smooth geomorphic surfaces, inflated soil horizons with limited exposed boulder fields, and elevations are consistent with presumed Bull Lake or older surface ages. A selected topographic profile measurement along MC5 with a maximum fault scarp height of ~75 m (Fig. 5a), yield a long-wavelength vertical separation of 68 ± 2 m for correlative lower and upper surfaces offset across multiple strands of the Bitterroot fault (Fig. 10b; profile C-C'). No in-situ age data yet exist for MC5 or any other Bull Lake glacial till deposits in Western Montana. If we extrapolate our slip rates results of 0.2–0.3 mm/yr and assume constant long-term rates, MC5 may yield a possible age of ~285–350 ka.

Rock Creek

Glacial Lake Missoula shorelines

Paleoshorelines provide another set of geomorphic strain marker to measure vertical separation across fault scarps offset by the Quaternary activity of the Bitterroot fault. Mapping using LiDAR-based slope index analyses identified multiple flights of wave-cut shorelines associated with Glacial Lake Missoula in the Bitterroot Valley (Plate 1; Figs. 11–12). Maximum elevations shorelines range between 4250 ft and 4230 ft along the Bitterroot Valley correlate to the Glacial Lake Missoula high stand that flooded the Bitterroot valley (Fig. 11). In the Rock Creek study site, east of Lake Como, maximum elevation shorelines are offset across a west-facing fault scarp interpreted as an antithetic strand of the Bitterroot fault (Fig. 12).

Topographic profile measurements yield vertical separation of 4.6 ± 1.6 m for offset shorelines between the footwall (4250 ft) and hanging wall (4230 ft) correlative surfaces across the west-dipping fault, with its uncertainty based on the map correlation of maximum elevation shorelines (Fig. 10c, profile *D-D').* Fault dips 70–80° to the East based on topographic relations of the mapped trace of the antithetic fault (Figs. 4 and 12). These maximum elevation shorelines of Glacial Lake Missoula are mapped near Lake Como Dam and inset into the youngest dated Pinedale glacial moraine deposits of S1-Qgty (~15.0 ka; Figs. 7 and 12). Our age results of ~15 ka represents a maximum age for the timing of highstand shoreline formation, broadly consistent with published estimates of the youngest dated Glacial Lake Missoula sediments associated with deep lake filling sequence that occurred prior to 13.4–13.7 ka before drainage (Smith et al., 2018). Rate calculations using an age range of 15.0 ± 0.4 ka and 15.4 ± 0.4 ka yield a fault slip rate of 0.20–0.44 mm/yr (Table 2).

Ward Creek Fan

Young Pinedale age glacial debris fan: S1 (Qdfy)

In the Ward Creek study site, north of Lake Como, the Bitterroot fault offsets young Pinedale-age glacial debris fan deposits S1 (Qgdfy) (Plate 1; Fig. 8). Fault lineaments mapped across the Ward Creek Fan complex consists of the main fault trace as NNE-SSW-trending east-facing fault scarp that offsets E-W sloping debris fan surface S1 (Figs. 6c and 8). A mapped secondary east-facing fault scarp is inferred to offset S1 as a local footwall fault splay to the Bitterroot fault (Figs. 8 and 10d). Topographic profile measurements yield a total vertical separation 2.4 ± 0.1 m for correlative surfaces S1 offset across both the main fault scarp and its fault splay (Fig. 10d, profile *E-E'*). Topographic constraints of the fault geometry near the Ward Creek Fan area indicate the main trace of the fault dips 45–60° to the East (Figs. 4 and 8). We assume the dip of the secondary fault strand is similar to the main fault trace. Rate calculations using an age range of 16.6 ± 0.4 ka and 17.1 ± 0.5 ka for S1 yield a fault slip rate of 0.15–0.23 mm/yr (Table 2).

Middle-aged glacial debris fan: S2 (Qdfm)

The Bitterroot fault offsets an older glacial debris fan deposits S2 (Qdfm) within the Ward Creek Fan complex (Plate 1; Figs. 6e and 8). S2 is characterized as the most extensive debris fan deposits with >500 m-long treads in the correlative hanging wall and footwall offset surfaces. The main trace of the Bitterroot fault across surface S2 consists of a well-exposed and continuous east-main facing scarp with no significant fault splays. Topographic profile measurements yield a vertical separation of 4.5 ± 0.1 m for correlative S2 surfaces offset by the fault scarp (Fig. 10e, profile *F-F'*). The fault dips 45–60°E to the East (Figs. 4 and 8). Rate calculations using age range of 62.8 ± 1.7 ka and 69.9 ± 2.2 ka for S2 yield a fault slip rate of 0.09–0.11 mm/yr (Table 2). Exposure model ages and resulting slip rates calculations for S2 include a larger degree of uncertainty compared to other study sites given its apparent complex depositional history of multiple debris flow sequences, inheritance, and/or post-surface modification.

Slip rate summary for the Bitterroot fault

Fault slip rates on the Bitterroot fault range between 0.1 mm/yr and 0.3 mm/yr associated with the main fault strand of the Bitterroot fault (Fig. 13; Table 2). At Lake Como, an offset young Pinedale moraine (MC2; Figs. 7 and 10a) yield a slip rate of 0.2–0.3 mm/yr. At the Ward Creek Fan, offset glacial debris fans (S1–S2; Figs. 8 and 10d–e) yield slip rates than range between 0.1 mm/yr (S2) and 0.2 mm/yr (S1). Our results indicate possible higher rates near Lake Como (0.2–0.3 mm/yr) compared to the Ward Creek Fan (0.1–0.2 mm/yr) further north (Fig. 13). However, the rates broadly overlap between the two study sites, which would yield an along-strike average of 0.2 ± 0.1 mm/yr for the southern section of the Bitterroot fault (Fig. 13). Our lowest slip rate site (0.1 mm/yr) in the Ward Creek Fan (S2; Figs. 8 and 13) may underestimate slip rates for the Bitterroot fault because of the larger degree of uncertainty in the age results due to inferred complex exposure history and/or post-surface modification (Fig. 9d). Our preferred along-strike average slip rate for the Bitterroot fault is 0.2–0.3 mm/yr (0.25 ± 0.05 mm/yr).

Slip rates on the antithetic fault strand of the Bitterroot fault are 0.2–0.4 mm/yr from offset Glacial Lake Missoula high stand shorelines at the Rock Creek study site (Figs. 12 and 13; Table 2). Equal slip rates partitioned on both the main fault strand (0.2–0.3 mm/yr) and antithetic fault strand (0.2–0.4mm/yr) of the Bitterroot fault are consistent with our structural framework interpretation (Fig. 4). Total slip and net extension accommodated on the long-wavelength hanging wall block (east of the antithetic fault) cannot exceed the total budget of 0.2–0.3 mm/yr. Fault block kinematics based on our slip rates results either dictate local differential deformation near the antithetic fault (e.g., east-directed hanging wall rotation) due to slip vectors as a high angle fault (Fig. 4a); or uniform fault-bounded block displacement (e.g., down-dropping of a graben) due to lateral slip vectors at depth as a low angle fault (Fig. 4b). Either fault model yields permissible solutions and fault block kinematics that can be tested with further detailed mapping of Bitterroot fault hanging wall strata along the Bitterroot Valley.

Regional strain rates for the Bitterroot valley.

Geodetic data indicate <2 mm/yr of extension rate across the Bitterroot valley (Payne et al., 2012; Schmeelk et al., 2017). A comparison of geodetic and geologic extension rates reveals the percentage of the geodetic rate accounted for by slip on the fault system, and the degree of slip partitioning. Our preferred geological extension rates of 0.1–0.3 mm/yr for the Bitterroot fault (Table 2) is lower than published geodetic extension rates (1-2 mm/yr; Schmeelk et al., 2017). However, geodetic rates for southwest Montana are derived from only one site within a poorly constrained region in the Intermountain West. We cannot exclude the possibility that additional unidentified Quaternary faults west of the LiDAR coverage may exist (Figs. 2 and 12), which, if present, would contribute to larger strain rates.

10. IMPLICATIONS FOR EARTHQUAKE POTENTIAL

New understanding of the fault activity along the Bitterroot fault provides constraints on the potential earthquake hazards to the Bitterroot-Missoula valleys (Figs. 1 and 2). Fault geometries frame the size of the potential earthquake. The Bitterroot fault extends ~100 km along the mountain front (Fig. 2). Empirical scaling relationships indicate that surface fault lengths of the Bitterroot fault could generate ~Mw 7.2 normal-fault earthquakes (Wells and Coppersmith, 1994; Stirling et al., 2013; https://earthquake.usgs.gov/scenarios/catalog/mt2016/)

Fault mapping and our results of geological slip rates suggest the Bitterroot fault is likely the primary seismogenic fault system within the Missoula-Bitterroot Valleys capable of releasing interseismic strain accumulation via surface-rupturing earthquakes. Paleoseismic records on the Bitterroot fault are yet unknown. We speculate the Bitterroot fault is likely characterized by millennia-timescale earthquake recurrence interval based on a loading slip rate of <1 mm/yr and the absence of historical earthquakes. Our NEHRP-funded study has identified multiple paleoseismic trench sites on the Bitterroot fault near Lake Como and Ward Creek study sites with the goal of developing a Holocene paleoearthquake chronology.

An earthquake and associated ground shaking on the Bitterroot could profoundly affect the Bitterroot valley and nearby Missoula metropolitan area, including critical infrastructure such as dams, canals, pipelines, transportation corridors, and power lines. New paleoseismic data are therefore needed to improve seismic source characterization of the Bitterroot to better understand the hazard. In addition, improved constraints of the deeper Bitterroot fault geometry are needed to address the possibility of a low angle seismogenic fault. An earthquake scenario on a low angle fault would suggest a larger seismogenic width and seismic hazard with an earthquake Mw > 7.2.

Our results provide the first in-situ age data and slip rates for seismic source characterization of the Bitterroot fault. This study builds on the previous work by Stickney and Lonn (2018) to reevaluate existing regional seismic source models for Western Montana. Our findings reinforce the need to include the Bitterroot fault in the National Seismic Hazards Maps as a seismogenic source for the Bitterroot-Missoula valleys, that could produce up to ~100 km long fault rupture along the Bitterroot Valley.

Acknowledgments. This material is based upon work supported by the U.S. Geological Survey under Grant No. G20AP00047 and received financial support from the Montana Bureau of Mines and Geology (MBMG). We would like to particularly Petr Yakovlev who wrote the original project proposal, and Alan Hidy at the CAMS, Lawrence Livermore National Lab for processing the Beryllium and AMS lab analytical results. We thank lab assistance from Connie Thompson, Kristina Okonski, and Jesse Mosolf, and GIS support from Yiwen Li, Susan Smith, Paul Thale, and Iris Smith at the MBMG. We also thank many fruitful discussions and insights on the project results with Ryan Gold, Chris DuRoss, and Alexandra Hatem from the USGS, and Ralph Klinger, Sylvia Nocovich, and Colin Chupick from the U.S. Bureau of Reclamation.

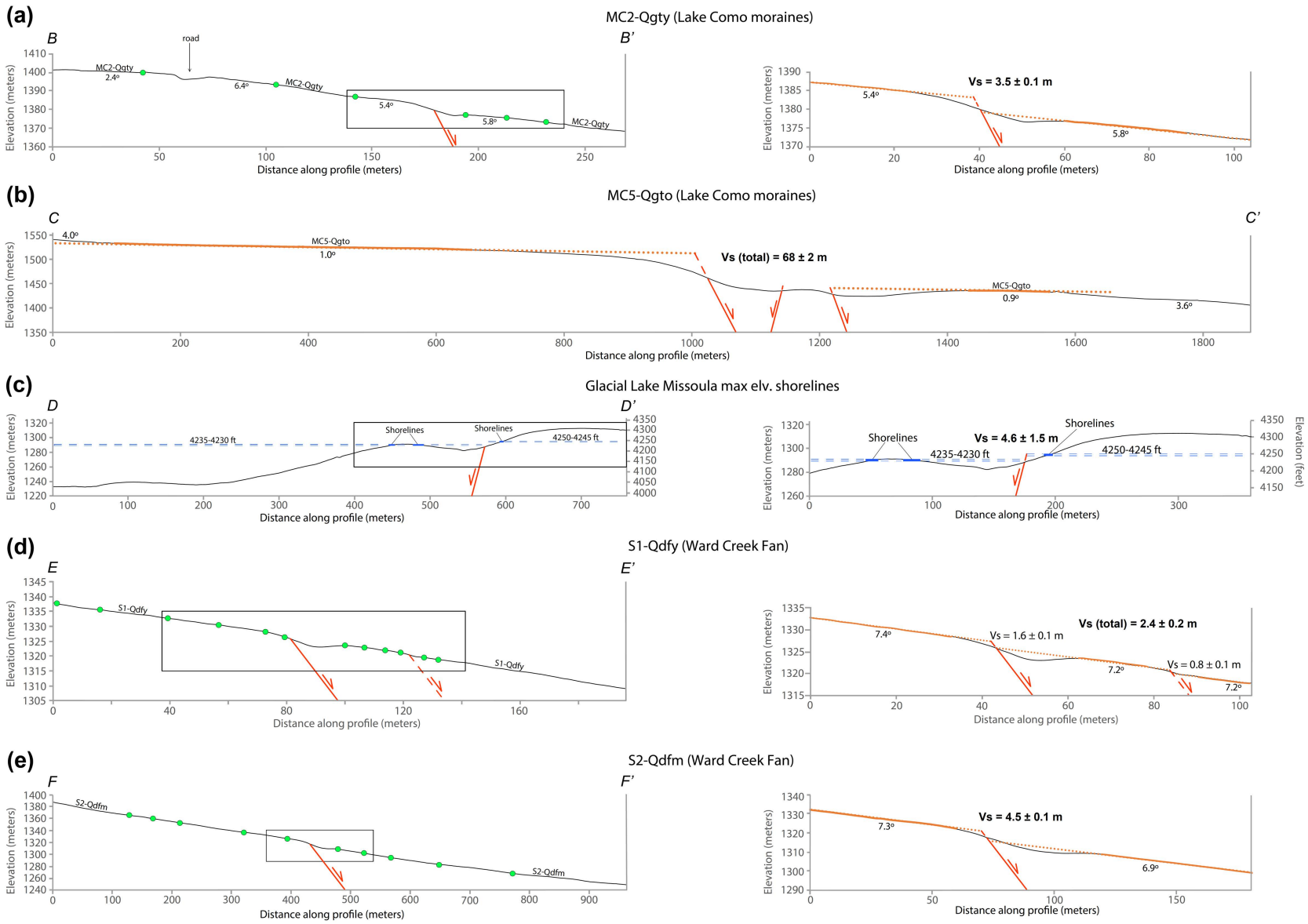

Figure 10. Vertical separation measurements (Vs) for multiple sites across the Bitterroot fault based on LiDAR-based regression slope topographic profiles of correlative hanging wall and footwall surfaces. a) Surface MC2 (Qgty) at Lake Como; b) Surface MC5 (Qgto) at Lake Como; c) Glacial Lake Missoula high stand shorelines at Rock Creek; d) Surface S1 (Qdfy) at Ward Creek Fan; e) Surface S2 (Qdfm) at Ward Creek Fan. See Figures 7, 8, and 12 for profile locations.

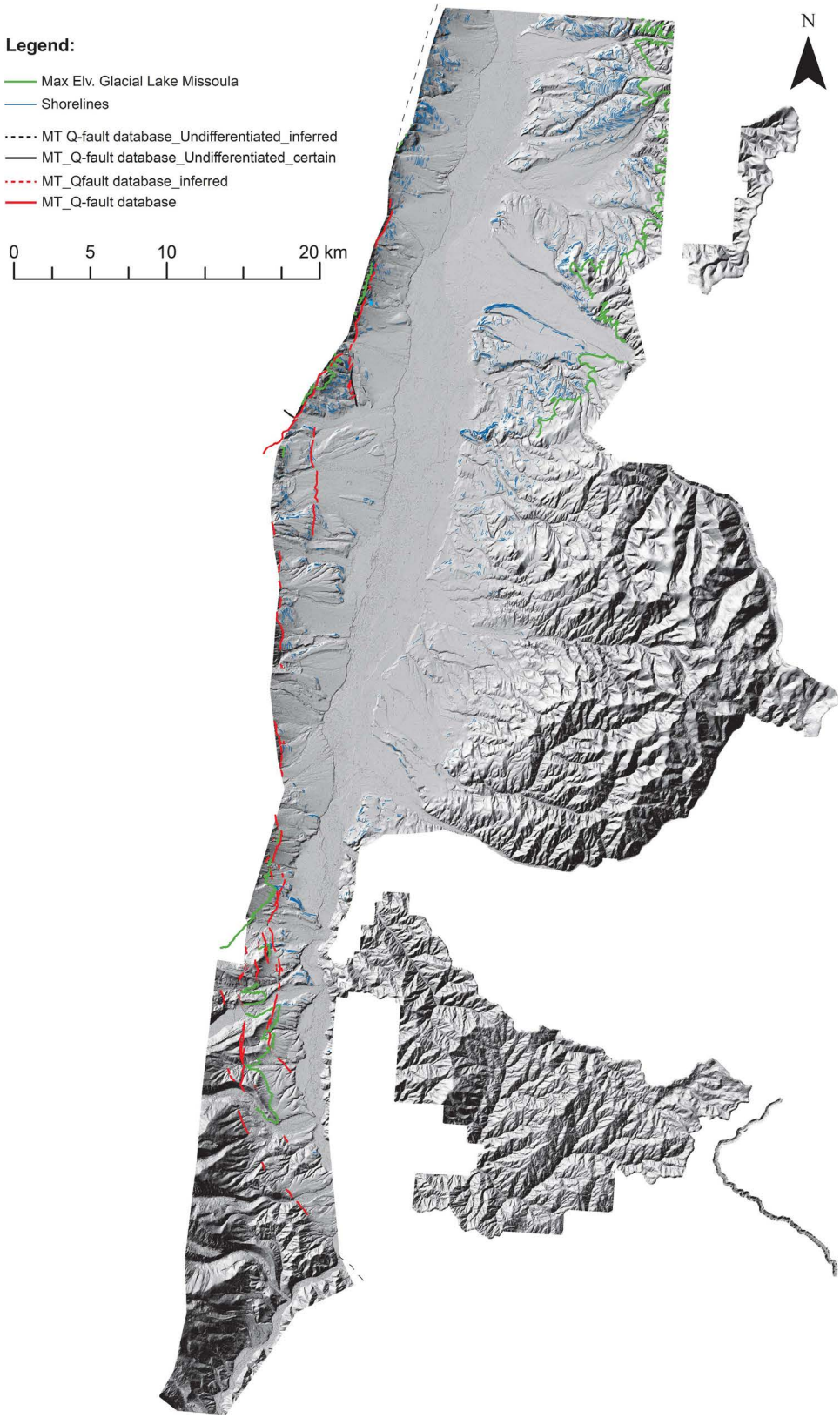

Figure 11. Compilation of mapped shorelines (blue) and Quaternary fault scarps (red) in the Bitterroot Valley using available LiDAR data, showing the maximum Elevation of Glacial Lake Missoula (green) that ranges between 4250 ft and 4230 ft. Note many shorelines demonstrate vertical offset across the Bitterroot fault.

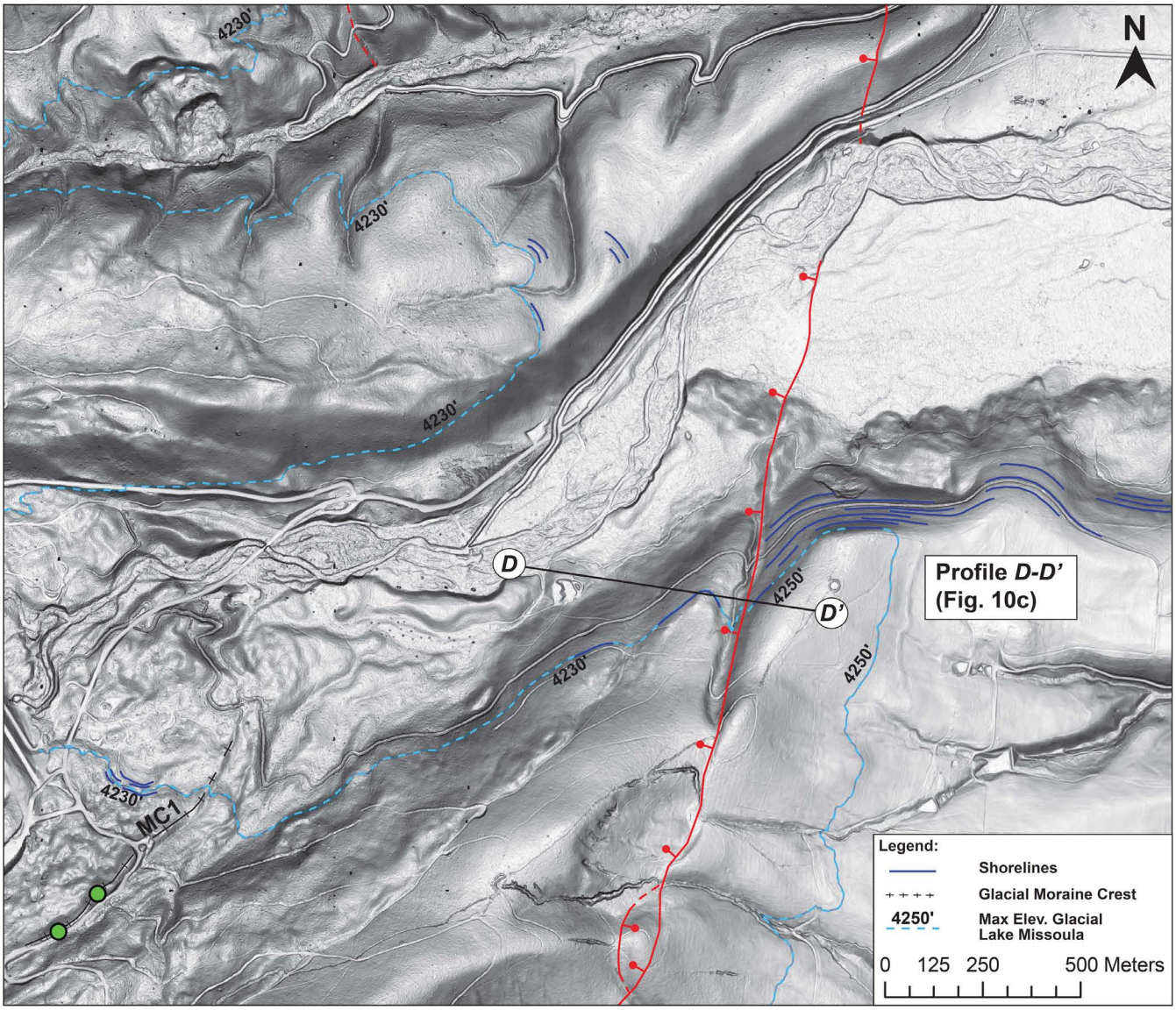

Figure 12. Detailed map of the Rock Creek study site showing antithetic fault strand of the Bitterroot fault and offset Glacial Lake Missoula shorelines. Mapping of the maximum elevation shorelines indicates a vertical separation between the footwall (4250 ft) and hanging wall (4230 ft) correlative surfaces across the west-dipping fault (see profile D-D' in Figure 10c). The same shorelines are mapped inset into Lake Como moraine crest, MC1, dated at ~15 ka. Base map is LiDAR slope hillshade DEM. See Figure 3 for location. Age results are shown in Table 1 and Figure 9.

TABLE 2. Vertical separation, extension, and fault slip rates for the Bitterroot fault.

	separation (m) Terrace	Min surface age (ka)	Max surface age (ka)	Fault dip (degrees)	Vert. separation rate (mm/yr)	Extension rate (mm/yr)	Fault slip rate (mm/yr)
Lake Como							
MC2 - Pinedale moraine	3.5 ± 0.1	16.4 ± 0.6	16.8 ± 0.6	62.5 ± 7.5	0.20–0.23	0.14–0.16	**0.21–0.28**
Rock Creek							
Glacial Lake Missoula shorelines	4.6 ± 1.5	15.0 ± 0.4	15.4 ± 0.4	75 ± 5	0.19–0.42	0.07–0.29	**0.20–0.44**
Ward Creek Fan							
S1 - Pinedale debris fan	2.4 ± 0.2	16.6 ± 0.4	17.1 ± 0.5	52.5 ± 7.5	0.13–0.16	0.07–0.16	**0.15–0.23**
S2 - Medium-aged debris fan	4.5 ± 0.1	62.8 ± 1.7	69.9 ± 2.2	52.5 ± 7.5	0.06–0.08	0.04–0.08	**0.09–0.11**

Note: Measured values of vertical separation, fault dip, and range of surface ages for offset marker units. Using these parameters, we calculated vertical separation rates, extension rate, and fault slip rates with corresponding uncertainties, which are based on the maximum and minimum possible values in the rate calculation.

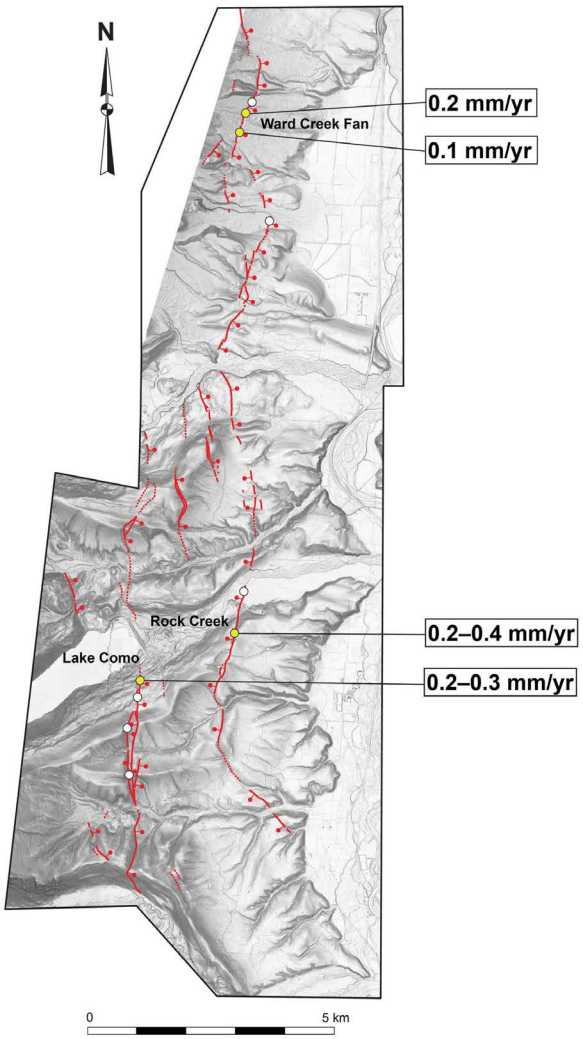

Figure. 13. Slip rates distribution map along the southern Bitterroot fault showing results from our study sites (yellow), and locations of forthcoming and future slip rate sites (white). Rates on the main east-dipping fault strand range between 0.1–0.3 mm/yr which yield an along strike average of 0.2 ± 0.1 mm/yr (Table 2). Our preferred along-strike slip rate average is 0.2–0.3 mm/yr, if we exclude the low slip rate site of 0.1 mm/yr in the Ward Creek Fan area (see text for details). Slip rates on the antithetic west-dipping fault are 0.2-0.4 mm/yr, which broadly overlap with the rates on the main strand of 0.2–0.3 mm /yr.

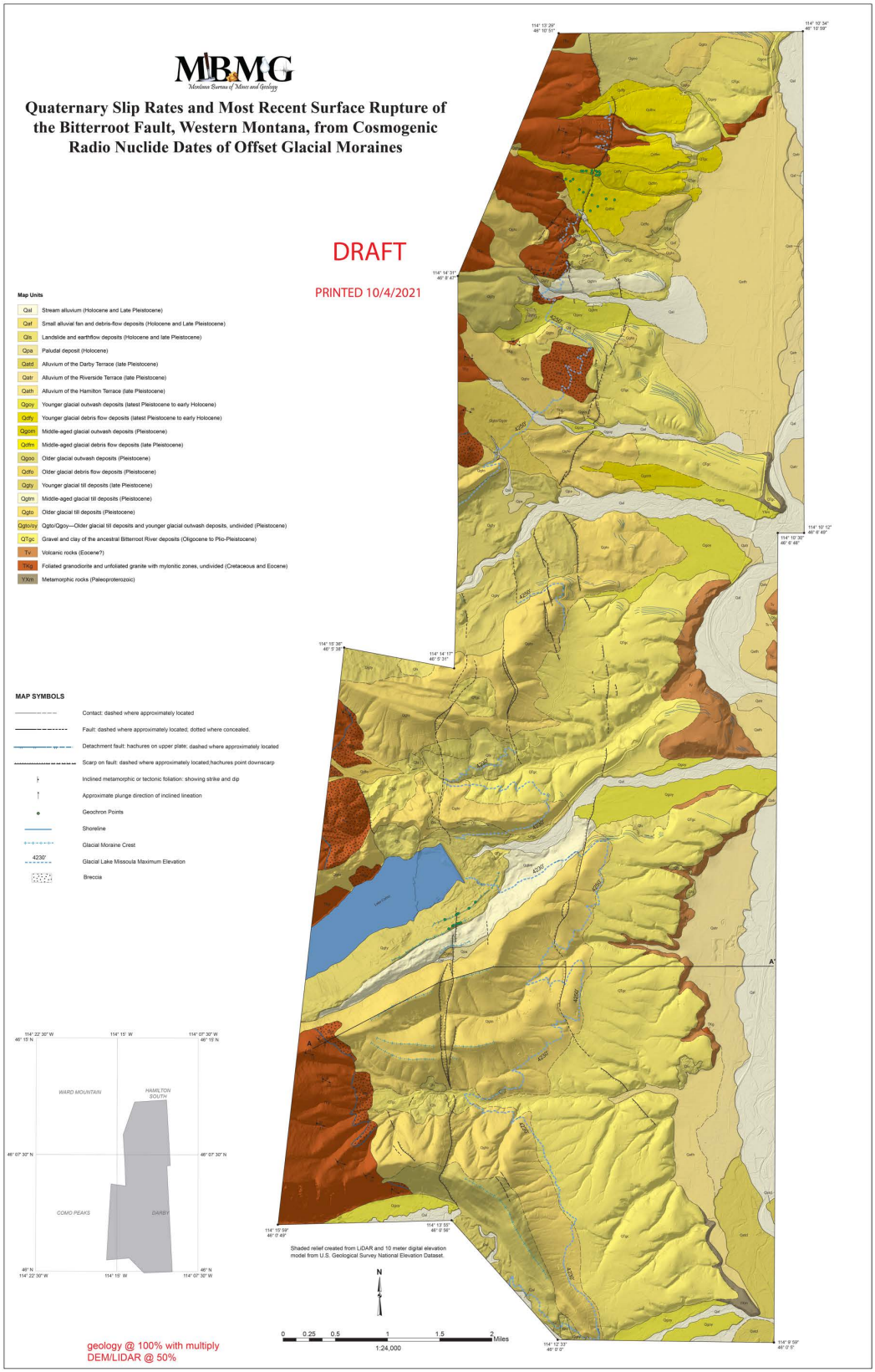

Plate 1. Geologic Map of the Southern Bitterroot map areas. See Figure 2 for location. Cross section along transect A-A' shown in Figure 4.

References

Arabasz, W.J., and Smith, R.B., 1981, Earthquake prediction in the Intermountain seismic belt—An intraplate extensional regime, in Earthquake prediction: An international review, Simpson, D.W., and Richards, P.G., eds., vol. 1, American Geophysical Union, Washington, D.C., p. 248–258, doi: 10.1029/ME004p0248.

Balco, G., Stone, J.O., Lifton, N.A., Dunai, T.J., 2008, A complete and easily accessible means of calculating surface exposure ages or erosion rates from 10Be and 26Al measurements. Quaternary Geochronology 3, 174–195.

Barkman, P.E., 1984, A reconnaissance investigation of active tectonism in the Bitterroot Valley, western Montana. M.S. thesis. Missoula: University of Montana. 85 pp.

Berg, R. B. and Lonn, J. D. 1996. Preliminary geologic map of the Nez Perce Pass 30 x 60 minute quadrangle, Montana. Open-File Report 339. Butte: Montana Bureau of Mines and Geology. Map scale 1:100,000.

Cartier, K. D. W. 1984. Sediment, channel morphology, and streamflow characteristics of the Bitterroot River drainage basin, southwestern Montana. M.S. thesis. Missoula: University of Montana. 191 pp.

De Polo, C.M., 1994, The Maximum background earthquake for the Basin and Range Province, western North America: Bulletin of the Seismological Society of America, v. 84, no. 2, p. 466–472.

Duxbury, J., Bierman, P.R., Portenga, E.W., Pavich, M.J., Southworth, S., Freeman, S.P., 2015, Erosion rates in and around Shenandoah National Park, Virginia, determined using analysis of cosmogenic 10Be. American Journal of Science 315, 46–76.

Foster, D.A., Schaferb, C., Fanning, C.M. and Hyndman, D.W., 2001, Relationships between crustal partial melting, plutonism, orogeny, and exhumation: Idaho–Bitterroot batholith: Tectonophysics, v. 342, p. 313-350.

Foster, D.A., and Raza, A., 2002, Low-temperature thermochronological record of exhumation of the Bitterroot metamorphic core complex, northern Cordilleran Orogen, Tectonophysics, Volume 349, Issues 1–4, 23-36.

Frankel, K. F., S. K. S. Brantley, J. F. Dolan, R. C. Finkel, R. E. Klinger, J. R. Knott, M. N. Machette, L. A. Owen, F. M. Phillips, J. L. Slate, and B. P. Wernicke, 2007, Cosmogenic 10Be and 36Cl geochronology of offset alluvial fans along the northern Death Valley fault zone: Implications for transient strain in the eastern California shear zone, Journal of Geophysical Research, 112, B06407, doi:10.1029/2006JB004350.

Gosse, J.C. and Phillips, F.M., 2001, Terrestrial in situ cosmogenic nuclides: theory and application: Quaternary Science Reviews, v. 20, p. 1475-1560.

Hatem, A.E., Collett, C.M., Gold, R.D., Briggs, R.W., Angster, S.A., Field, E.H., Anderson, M., Ben Horin, J.Y., Dawson, T., DeLong, S., DuRoss, C., Thompson Jobe, J., Kleber, E., Knudsen, K.L., Koehler, R., Koning, D., Lifton, Z., Madin, I., Mauch, J., Morgan, M., Pearthree, P., Petersen, M., Pollitz, F., Scharer, K., Powers, P., Sherrod, B., Stickney, M., Wittke, S., and Zachariasen, J., 2021, Earthquake geology inputs for the National Seismic Hazard Model (NSHM) 2023, version 1.0: U.S. Geological Survey, doi: 10.5066/P918XCUU

Hidy, A., Gosse, J.C., Pederson, J.L., Mattern, J.P., Finkel, R.C., 2010, A geologically constrained Monte Carlo approach to modeling exposure ages from profiles of cosmogenic nuclides: An example from Lees Ferry, Arizona: Geochemistry Geophysics Geosystems, v. 11, Q0AA10, p. 1–18, doi:10.1029/2010GC003084.

Hyndman, D.W., 1980. Bitterroot dome–Sapphire tectonic block, an example of a plutonic core– gneiss–dome complex with its detached suprastructure, *in* Crittenden, M.D., Coney, P.J., Davis, G.H. (eds.), Cordilleran Metamorphic Core Complexes: Geological Society of America Memoir, vol. 153, p. 427– 443.

Heyman, J., 2014, Paleoglaciation of the Tibetan Plateau and surrounding mountains based on exposure ages and ELA depression estimates: Quaternary Science Reviews, v. 91, p. 30–41, doi:10.1016/j.quascirev.2014.03.018.

Jackson, L.E., Phillips, F.M., Shimamura, K., Little, E.C., 1997. Cosmogenic 36Cl dating of the Foothills erratics train, Alberta, Canada. Geology 25, 195–198.

Kohl, C.P., and Nishiizumi, K., 1992, Chemical isolation of quartz for measurement of in situ–produced cosmogenic nuclides: Geochimica et Cosmochimica Acta, v. 56, p. 3583–3587, doi:10.1016/0016-7037(92)90401-4.

Konizeski, R. L., 1958, Pliocene vertebrate fauna from the Bitterroot Valley, Montana, and its stratigraphic significance, Geological Society of America Bulletin 69: 325-345.

Lal, D. (1991), Cosmic ray labeling of erosion surfaces in situ nuclide production rates and erosion models, Earth Planetary Science Letters, 104, p 424-439.

Licciardi, J., 2000, Alpine Glacier and Pluvial Lake Records of Late Pleistocene Climate Variability in the Western United States [Ph.D. thesis]: Corvallis, Oregon, Oregon State University, 155 p.

Licciardi, J.M., and Pierce, K.L., 2008, Cosmogenic exposure-age chronologies of Pinedale and Bull Lake glaciations in greater Yellowstone and the Teton Range, USA, Quaternary Science Reviews, Volume 27, issues 7–8, 814-831.

Lonn, J. D. and Berg, R. B., 1996, Preliminary geologic map of the Hamilton 30 x 60 minute quadrangle, Montana. Open-File Report 340. Butte: Montana Bureau of Mines and Geology. Map scale 1:100,000.

Lonn, J.D., and Sears, J.W., 2001, Geology of the Bitterroot Valley, shaded relief: Montana Bureau of Mines and Geology Open-File Report 441-C, 1 sheet, scale 1:48,000.

Margold, M., Gosse, J., Hidy, A., Woywitka, R., Young, J., Froese, D., 2019, Beryllium-10 dating of the Foothills Erratics Train in Alberta, Canada, indicates detachment of the Laurentide Ice Sheet from the Rocky Mountains at ~15 ka, Quaternary Research, v. 92, 1-14. 10.1017/qua.2019.10.

Mason, D.B., 1996, Earthquake magnitude potential of the Intermountain Seismic Belt, USA, from surface-parameter scaling of late quaternary faults: Bulletin of the Seismological Society of America, v. 86, no. 5, p. 1487–1506.

McMurtrey, R. G., Konizeski R. L., Johnson, M. V., and Bartells, J. H. 1972. Geology and water resources of the Bitterroot Valley, southwestern Montana. U.S. Geological Survey Water Supply Paper 1889. 80 p. Map scale 1:125,000.

Myers, W.B., and Hamilton, W., 1964, Deformation accompanying the Hebgen Lake earthquake of August 17, 1959, The Hebgen Lake, Montana, Earthquake of August 17, 1959 (v. 435, p. 55–98): Geological Survey Professional Paper: Washington, D.C., U.S. Government Printing Office.

Norbeck, P. M. 1980. Preliminary evaluation of deep aquifers in the Bitterroot and Missoula valleys in western Montana. Open File Report 46. Butte: Montana Bureau of Mines and Geology. 15 pp.

Payne, S.J., McCaffrey, R., King, R.W., and Kattenhorn, S.A., 2012, A new interpretation of deformation rates in the Snake River Plain and adjacent Basin and Range regions based on GPS measurements: Geophysical Journal International, v. 189, p. 101–122.

Petersen, M.D., Moschetti, M.P., Powers, P.M., Mueller, C.S., Haller, K.M., Frankel, A.D., Zeng, Y., Rezaeian, S., Harmsen, S.C., Boyd, O.S., Field, E.H., Chen, R., Luco, N., Wheeler, R.L., and

others, 2014, Seismic-hazard maps for the conterminous United States, 2014: U.S. Geological Survey Scientific Investigations Map 3325.
Pierce, K.L., 2004, Pleistocene glaciations of the Rocky Mountains, Developments in Quaternary Sciences, Elsevier, v. 1, 63-76.
A.R. Gillespie, S.C. Porter, B.F. Atwater (Eds.), The Quaternary Period in the United States: Developments in Quaternary Science, vol. 1, Amsterdam, Elsevier (2004), pp. 63-76
U.S. Geological Survey and Montana Bureau of Mines and Geology, 2006, Quaternary fault and fold database for the United States, accessed 4/17/2018, from USGS web site: http//earthquake.usgs.gov/hazards/qfaults/.
U.S. Geological Survey, Montana Earthquake Scenario Catalog, accessed 10/27/2021 from USGS web site: https://earthquake.usgs.gov/scenarios/catalog/mt2016/.
Ross, C.P. 1952. The eastern front of the Bitterroot Range, Montana: U.S. Geological Survey Bulletin 974, p. 135-175, map scale 1:125,000.
Sbar, M.L., Barazangi, M., Dorman, J., Scholz, C.H., and Smith, R.B., 1972, Tectonics of the intermountain seismic belt, western United States: Micro earthquake seismicity and the composite fault place solutions: Geological Society of America Bulletin, v. 83, no. 1, p. 13–28, doi: 10.1130/0016-7606(1972)83[13:TOTISB]2.0.CO;2.
Schmeelk, D., Bendick, R., Stickney, M., and Bomberger, C., 2017, Kinematic evidence for the effect of changing plate boundary conditions on the tectonics of the northern US Rockies: Tectonics, v. 36, p. 1090–1102, doi: https://doi.org/10.1002/2016TC004427
Smith, R.B., and Arabasz, W.J., 1991, Seismicity of the intermountain seismic belt, in Neotectonics of North America, Slemmons, D.B., Engdahl, E.R., Zoback, M.D., and Blackwell, D.D., eds., Geological Society of America, 185–228, doi: 10.1130/DNAG-CSMS-NEO.185
Smith, L., 2006, Altitude of the Bedrock Surface in the Bitterroot Valley: Missoula and Ravalli Counties, Montana. Montana Ground-Water Assessment Atlas 4, Part B, Map 5. Butte: Montana Bureau of Mines and Geology.
Smith, L., Sohbati, R., Buylaert, J-P., Lian, O.B., Murray, A., Jain, M., 2018, Timing of lake-level changes for a deep last-glacial Lake Missoula: optical dating of the Garden Gulch area, Montana, USA, Quaternary Science Reviews, v. 183, 23-35.
Stickney, M., 2015, Seismicity within and adjacent to the eastern Lewis and Clark line, west-central Montana: Northwest Geology v. 44, p. 19-36.
Stickney, M.C., and Lonn, J.D., 2018, Investigation of late Quaternary Fault scarps along the Bitterroot Fault in western Montana: Montana Bureau of Mines and Geology Report of Investigation 24, 16 p, 2 plates.
Stirling, M., Goded, T., Berryman, K., and Litchfield, N., 2013, Selection of Earthquake Scaling Relationships for Seismic-Hazard Analysis, Bulletin of the Seismological Society of America, v. 103, 6, 2993-3011, doi: 10.1785/0120130052
Stone, J.O., 2000, Air pressure and cosmogenic isotope production: Journal of Geophysical Research, v. 105, p. 23,753–23,759, doi:10.1029/2000JB900181.
Vermeesch, P., 2012. On the visualisation of detrital age distributions. Chemical Geology, v.312-313, 190-194, doi: 10.1016/j.chemgeo.2012.04.021
Weber, W.M. 1972. Correlation of Pleistocene glaciation in the Bitterroot Range, Montana, with fluctuations of glacial Lake Missoula. Memoir 42. Butte: Montana Bureau of Mines and Geology. 42 pp.

Wells, D. L. and Coppersmith, K. J., 1994, New empirical relationships among magnitude, rupture length, rupture width, rupture area, and surface displacement: Bulletin of the Seismological Society of America, v. 84, no. 4, p. 974-1002.

Witkind, I.J., Myers, W.B., Hadley, J.B., Hamilton, W., and Fraser, G.D., 1962. Geologic features of the earthquake at Hebgen Lake, Montana, August 17, 1959: Bulletin of the Seismological Society of America, v. 52, no. 2, p. 163–180.

Witkind, I.J., 1964, Reactivated faults north of Hebgen Lake, The Hebgen Lake, Montana, Earthquake of August 17, 1959 (vol. 435, p. 37–50): Geological Survey Professional Paper: Washington, D.C., U.S. Government Printing Office.

Supplemental File 1. Model parameters and data input for modeling cosmogenic nuclide ^{10}Be surface exposure dating using CRONUS Age Calculator.

CRONUS Age Calculator - Data input

Batch ID	Sample	Lat	Long	Elv (m)	Elv/Pressure handling flag	Sample thickness (cm)[a]	Sample density (g/cm3)[b]	Shield Correction[c]	Erosion rates (cm/yr)[d]	Date sample collection	Isotope	Mineral	Be10 Conc.	Error	Standard
	Ward Creek Fan:														
	S1-Lower (Qdfy)														
54	WCF-Qdfy-S1-lower-1	46.16152	-114.215608	1321	std	1	2.57	0.996478	0 / 0.0002	2020	Be-10	quartz	330078.2768	6407.248159	KNSTD
54	WCF-Qdfy-S1-lower-2	46.161483	-114.215093	1315	std	1	2.57	0.996817	0 / 0.0002	2020	Be-10	quartz	218492.1546	4375.701757	KNSTD
54	WCF-Qdfy-S1-lower-3	46.161692	-114.214868	1315	std	1	2.57	0.996804	0 / 0.0002	2020	Be-10	quartz	690483.573	9991.253068	KNSTD
54	WCF-Qdfy-S1-lower-4	46.161944	-114.215443	1323	std	1	2.57	0.959965	0 / 0.0002	2020	Be-10	quartz	274901.061	4958.767371	KNSTD
54	WCF-Qdfy-S1-lower-5	46.162041	-114.215004	1317	std	1	2.57	0.99636	0 / 0.0002	2020	Be-10	quartz	298276.2115	5328.345806	KNSTD
54	WCF-Qdfy-S1-lower-6	46.162061	-114.215653	1325	std	1	2.57	0.996981	0 / 0.0002	2020	Be-10	quartz	230636.0593	4664.240646	KNSTD
	Ward Creek Fan:														
	S1-Upper (Qdfy)														
54	WCF-Qdfy-S1-upper-1	46.162111	-114.216519	1335	std	1	2.57	0.99496	0 / 0.0002	2020	Be-10	quartz	230898.4748	4642.023484	KNSTD
54	WCF-Qdfy-S1-upper-2	46.161994	-114.217598	1348	std	1	2.57	0.996759	0 / 0.0002	2020	Be-10	quartz	244452.327	4892.820977	KNSTD
54	WCF-Qdfy-S1-upper-3	46.161917	-114.2182	1355	std	1	2.57	0.995886	0 / 0.0002	2020	Be-10	quartz	223523.3538	5289.774374	KNSTD
54	WCF-Qdfy-S1-upper-4	46.161944	-114.218611	1360	std	1	2.57	0.996257	0 / 0.0002	2020	Be-10	quartz	224820.1801	4539.623279	KNSTD
54	WCF-Qdfy-S1-upper-5	46.161755	-114.216547	1334	std	1	2.57	0.99278	0 / 0.0002	2020	Be-10	quartz	176165.3906	3532.384624	KNSTD
	Ward Creek Fan:														
	S2-Lower (Qdfm)														
58	WCF-Qdfm-S2-lower-1	46.158698	-114.216225	1310	std	1	2.57	0.996981	0 / 0.0002	2020	Be-10	quartz	1310826.191	20218.82544	KNSTD
58	WCF-Qdfm-S2-lower-2	46.158274	-114.21334	1280	std	1	2.57	0.996981	0 / 0.0002	2020	Be-10	quartz	1285181.112	19901.07275	KNSTD
58	WCF-Qdfm-S2-lower-3	46.158213	-114.211642	1267	std	1	2.57	0.996968	0 / 0.0002	2020	Be-10	quartz	947747.846	14295.30561	KNSTD
58	WCF-Qdfm-S2-lower-4	46.156498	-114.216332	1289	std	1	2.57	0.996969	0 / 0.0002	2020	Be-10	quartz	840718.4401	11886.1754	KNSTD
58	WCF-Qdfm-S2-lower-5	46.157164	-114.214925	1285	std	1	2.57	0.996981	0 / 0.0002	2020	Be-10	quartz	1385910.482	19536.94888	KNSTD
	Ward Creek Fan:														
	S2-Upper (Qdfm)														
58	WCF-Qdfm-S2-upper-1	46.159341	-114.21877	1344	std	1	2.57	0.996977	0 / 0.0002	2020	Be-10	quartz	790824.1104	11124.11507	KNSTD
58	WCF-Qdfm-S2-upper-2	46.160737	-114.220153	1373	std	1	2.57	0.996758	0 / 0.0002	2020	Be-10	quartz	966217.3548	17989.24779	KNSTD
58	WCF-Qdfm-S2-upper-3	46.160691	-114.221614	1384	std	1	2.57	0.996127	0 / 0.0002	2020	Be-10	quartz	291694.2867	5395.249434	KNSTD
58	WCF-Qdfm-S2-upper-4	46.160441	-114.220668	1374	std	1	2.57	0.996981	0 / 0.0002	2020	Be-10	quartz	833961.7162	14034.16989	KNSTD
58	WCF-Qdfm-S2-upper-5	46.159012	-114.217954	1333	std	1	2.57	0.994069	0 / 0.0002	2020	Be-10	quartz	1317388.847	20320.41003	KNSTD
	Lake Como Morraine:														
	MC1 (Qgty)														
57	LCS-Qgty-MC1-upper-1	46.057183	-114.236761	1355	std	1	2.57	0.989542	0 / 0.0002	2020	Be-10	quartz	208360.0312	4319.992433	KNSTD
57	LCS-Qgty-MC1-upper-2	46.057924	-114.234597	1345	std	1	2.57	0.998349	0 / 0.0002	2020	Be-10	quartz	192048.2846	3852.790069	KNSTD
57	LCS-Qgty-MC1-lower-3	46.058918	-114.232156	1329	std	1	2.57	0.998845	0 / 0.0002	2020	Be-10	quartz	215010.7245	4402.807248	KNSTD
57	LCS-Qgty-MC1-lower-4	46.05983	-114.23092	1327	std	1	2.57	0.998562	0 / 0.0002	2020	Be-10	quartz	209373.6448	4196.588083	KNSTD
57	LCS-Qgty-MC1-fault-5	46.058095	-114.234252	1346	std	1	2.57	0.998455	0 / 0.0002	2020	Be-10	quartz	204992.5209	4105.170905	KNSTD
	Lake Como Morraine:														
	MC2 (Qgty)														
57	LCS-Qgty-MC2-lower-1	46.056855	-114.233578	1366	std	1	2.57	0.997926	0 / 0.0002	2020	Be-10	quartz	225658.4867	5031.415896	KNSTD
57	LCS-Qgty-MC2-lower-2	46.056771	-114.233924	1367	std	1	2.57	0.998534	0 / 0.0002	2020	Be-10	quartz	191997.9871	3864.2781	KNSTD
57	LCS-Qgty-MC2-lower-3	46.056698	-114.234311	1373	std	1	2.57	0.996904	0 / 0.0002	2020	Be-10	quartz	224065.9626	4340.248394	KNSTD
57	LCS-Qgty-MC2-upper-4	46.056456	-114.234938	1380	std	1	2.57	0.998948	0 / 0.0002	2020	Be-10	quartz	230696.5105	4694.30873	KNSTD
57	LCS-Qgty-MC2-upper-5	46.05633	-114.235173	1387	std	1	2.57	0.998404	0 / 0.0002	2020	Be-10	quartz	297086.3593	6066.126402	KNSTD
57	LCS-Qgty-MC2-upper-6	46.055926	-114.235900	1395	std	1	2.57	0.997285	0 / 0.0002	2020	Be-10	quartz	254071.8333	4574.686848	KNSTD

[a] Sample thickness represents the total amount of material modelled for Be10 exposure dating that includes 1 ± 0.5 cm of bedrock (granodiorite-gneiss) sampled interval.

[b] Average measured density of boulder foliated biotite-muscovite granodiorite to gneiss samples (2.57 ± 0.1 g/cm3).

[c] Geometric shielding correction using CRONUS online calculator

[d] Assumed value of erosion rates for stabe and resistant foliated granodiorite boulders that have preserved glacial erosional surfaces.

Topographic Shielding Measurements

Sample	Strike of surface (azimuth°)	Dip of surface (°)	Azimuth (0-360°)	Inclination (0-90°)	Shield Correction
Ward Creek Fan:					
S1-Lower (Qdfy)					
WCF-Qdfy-S1-lower-1	281	10	0,45,90,135,170,210,230,270,335	2,2,2,3,3,5,9,18,10	0.996478
WCF-Qdfy-S1-lower-2	248	7	0,45,90,135,170,210,230,270,335	2,2,2,3,3,5,9,18,10	0.996817
WCF-Qdfy-S1-lower-3	328	10	0,45,90,135,170,210,230,270,335	2,2,2,3,3,5,9,18,10	0.996804
WCF-Qdfy-S1-lower-4	355	36	0,45,90,135,170,210,230,270,335	2,2,2,3,3,5,9,18,10	0.959965
WCF-Qdfy-S1-lower-5	139	10	0,45,90,135,170,210,230,270,335	2,2,2,3,3,5,9,18,10	0.99636
WCF-Qdfy-S1-lower-6	212	0	0,45,90,135,170,210,230,270,335	2,2,2,3,3,5,9,18,10	0.996981
Ward Creek Fan:					
S1-Upper (Qdfy)					
WCF-Qdfy-S1-upper-1	316	16	0,45,90,135,170,210,230,270,335	2,2,2,3,3,5,9,18,10	0.99496
WCF-Qdfy-S1-upper-2	350	13	0,45,90,135,170,210,230,270,335	2,2,2,3,3,5,9,18,10	0.996759
WCF-Qdfy-S1-upper-3	35	16	0,45,90,135,170,210,230,270,335	2,2,2,3,3,5,9,18,10	0.995886
WCF-Qdfy-S1-upper-4	11	17	0,45,90,135,170,210,230,270,335	2,2,2,3,3,5,9,18,10	0.996257
WCF-Qdfy-S1-upper-5	15	21	0,45,90,135,170,210,230,270,335	2,2,2,3,3,5,9,18,10	0.99278
Ward Creek Fan:					
S2-Lower (Qdfm)					
WCF-Qdfm-S2-lower-1	12	4	0,45,90,135,170,210,230,270,335	2,2,2,3,3,5,9,18,10	0.996981
WCF-Qdfm-S2-lower-2	24	2	0,45,90,135,170,210,230,270,335	2,2,2,3,3,5,9,18,10	0.996981
WCF-Qdfm-S2-lower-3	297	5	0,45,90,135,170,210,230,270,335	2,2,2,3,3,5,9,18,10	0.996968
WCF-Qdfm-S2-lower-4	49	6	0,45,90,135,170,210,230,270,335	2,2,2,3,3,5,9,18,10	0.996969
WCF-Qdfm-S2-lower-5	9	4	0,45,90,135,170,210,230,270,335	2,2,2,3,3,5,9,18,10	0.996981
Ward Creek Fan:					
S2-Upper (Qdfm)					
WCF-Qdfm-S2-upper-1	205	3	0,45,90,135,170,210,230,270,335	2,2,2,3,3,5,9,18,10	0.996977
WCF-Qdfm-S2-upper-2	34	13	0,45,90,135,170,210,230,270,335	2,2,2,3,3,5,9,18,10	0.996758
WCF-Qdfm-S2-upper-3	140	11	0,45,90,135,170,210,230,270,335	2,2,2,3,3,5,9,18,10	0.996127
WCF-Qdfm-S2-upper-4	66	2	0,45,90,135,170,210,230,270,335	2,2,2,3,3,5,9,18,10	0.996981
WCF-Qdfm-S2-upper-5	128	16	0,45,90,135,170,210,230,270,335	2,2,2,3,3,5,9,18,10	0.994069
Lake Como Morraine:					
MC1 (Qgty)					
LCS-Qgty-MC1-upper-1	68	21	0,45,80,110,130,160,210,240,250,265,280,340	3,3,2,4,11,18,12,10,11,0,10,7	0.989542
LCS-Qgty-MC1-upper-2	322	10	0,45,75,110,160,200,250,260,280,340	1,1,3,8,10,11,8,0,10,6	0.998349
LCS-Qgty-MC1-lower-3	191	9	0,45,90,135,180,230,265,280,340	3,1,5,8,10,6,0,8,7	0.998845
LCS-Qgty-MC1-lower-4	271	1	0,45,90,135,180,220,230,250,260,280,340	2,2,6,10,10,10,10,6,0,9,7	0.998562
LCS-Qgty-MC1-fault-5	341	8	0,45,75,110,160,200,250,260,280,340	1,1,3,8,10,11,8,0,10,6	0.998455
Lake Como Morraine:					
MC2 (Qgty)					
LCS-Qgty-MC2-lower-1	45	11	0,30,130,185,250,290,330	0,2,4,9,13,7,7	0.997926
LCS-Qgty-MC2-lower-2	113	9	0,30,120,180,250,290,340	0,1,4,9,9,9,7	0.998534
LCS-Qgty-MC2-lower-3	328	16	0,30,65,130,170,205,250,300,340	2,1,1,3,8,13,10,6,5	0.996904
LCS-Qgty-MC2-upper-4	3	0	0,30,50,90,130,190,240,280,340	4,0,2,4,5,8,10,9,7	0.998948
LCS-Qgty-MC2-upper-5	18	12	0,45,65,95,130,180,240,255,285,340	0,0,3,4,5,9,8,10,6,7	0.998404
LCS-Qgty-MC2-upper-6	201	14	0,45,90,135,180,225,265,280,340	0,0,4,6,8,10,0,10,8	0.997285

CRONUS Age Calculator - Age model results for zero erosion rate

Sample	Nuclide	St			Lm			LSDn		
		Age (yr)	Internal error	External error (yr)	Age (yr)	Internal error (yr)	External error (yr)	Age (yr)	Internal error	External error
Ward Creek Fan:										
S1-Lower (Qdfy)										
WCF-Qdfy-S1-lower-1	Be-10 (qtz)	24633	481	2016	23718	463	1848	23868	466	1491
WCF-Qdfy-S1-lower-2	Be-10 (qtz)	16342	329	1337	16011	322	1248	16209	326	1014
WCF-Qdfy-S1-lower-3	Be-10 (qtz)	52106	764	4240	49773	729	3849	49962	732	3073
WCF-Qdfy-S1-lower-4	Be-10 (qtz)	21236	385	1730	20592	373	1597	20764	377	1288
WCF-Qdfy-S1-lower-5	Be-10 (qtz)	22318	401	1818	21583	388	1673	21747	391	1348
WCF-Qdfy-S1-lower-6	Be-10 (qtz)	17118	348	1402	16746	340	1306	16935	344	1061
Ward Creek Fan:										
S1-Upper (Qdfy)										
WCF-Qdfy-S1-upper-1	Be-10 (qtz)	17039	344	1395	16670	337	1300	16853	340	1055
WCF-Qdfy-S1-upper-2	Be-10 (qtz)	17831	358	1460	17417	350	1358	17584	353	1100
WCF-Qdfy-S1-upper-3	Be-10 (qtz)	16225	386	1343	15899	378	1255	16069	382	1026
WCF-Qdfy-S1-upper-4	Be-10 (qtz)	16250	329	1330	15923	323	1242	16091	326	1007
WCF-Qdfy-S1-upper-5	Be-10 (qtz)	13026	262	1065	12803	258	997	12990	261	812
Ward Creek Fan:										
S2-Lower (Qdfm)										
WCF-Qdfm-S2-lower-1	Be-10 (qtz)	100490	1590	8295	95522	1509	7492	95728	1512	5980
WCF-Qdfm-S2-lower-2	Be-10 (qtz)	100851	1602	8327	95870	1521	7521	96187	1526	6011
WCF-Qdfm-S2-lower-3	Be-10 (qtz)	74641	1147	6116	71261	1094	5550	71635	1100	4441
WCF-Qdfm-S2-lower-4	Be-10 (qtz)	64936	933	5297	62201	893	4822	62535	898	3854
WCF-Qdfm-S2-lower-5	Be-10 (qtz)	108543	1572	8951	102901	1489	8058	103133	1492	6420
Ward Creek Fan:										
S2-Upper (Qdfm)										
WCF-Qdfm-S2-upper-1	Be-10 (qtz)	58442	834	4759	56112	800	4342	56349	804	3466
WCF-Qdfm-S2-upper-2	Be-10 (qtz)	70045	1327	5786	66836	1265	5252	66888	1266	4208
WCF-Qdfm-S2-upper-3	Be-10 (qtz)	20726	385	1690	20118	374	1562	20244	376	1258
WCF-Qdfm-S2-upper-4	Be-10 (qtz)	60251	1029	4941	57839	988	4511	58002	990	3611
WCF-Qdfm-S2-upper-5	Be-10 (qtz)	99478	1573	8209	94585	1494	7416	94712	1496	5915
Lake Como Morraine:										
MC1 (Qgty)										
LCS-Qgty-MC1-upper-1	Be-10 (qtz)	15245	317	1250	14975	312	1170	15146	315	951
LCS-Qgty-MC1-upper-2	Be-10 (qtz)	14031	282	1148	13811	278	1076	14017	282	877
LCS-Qgty-MC1-lower-3	Be-10 (qtz)	15903	327	1303	15590	320	1217	15782	324	990
LCS-Qgty-MC1-lower-4	Be-10 (qtz)	15513	312	1269	15222	306	1186	15414	310	964
LCS-Qgty-MC1-fault-5	Be-10 (qtz)	14968	301	1224	14720	296	1147	14900	300	932
Lake Como Morraine:										
MC2 (Qgty)										
LCS-Qgty-MC2-lower-1	Be-10 (qtz)	16239	364	1338	15910	356	1250	16082	360	1018
LCS-Qgty-MC2-lower-2	Be-10 (qtz)	13789	278	1128	13570	274	1057	13740	277	859
LCS-Qgty-MC2-lower-3	Be-10 (qtz)	16054	312	1311	15733	306	1224	15897	309	991
LCS-Qgty-MC2-upper-4	Be-10 (qtz)	16409	335	1344	16074	328	1254	16233	332	1017
LCS-Qgty-MC2-upper-5	Be-10 (qtz)	21053	432	1727	20417	419	1595	20547	422	1289
LCS-Qgty-MC2-upper-6	Be-10 (qtz)	17901	324	1457	17479	316	1354	17621	319	1092

St: Time-independent scaling age model by Stone et al. (2000), which is based on Lal (1991).
Lm: Time-dependent scaling age model by Lal/Stone that accounts for geomagnetic field variations.
LSDn: Nuclide-dependent scaling age model by Lifton-Stato-Dunai.

Age results generated by CRONUS-Earth online calculators, Balco et al. (2008).
https://hess.ess.washington.edu/
version 3

CRONUS Age Calculator- Age model results for 2 mm/ka erosion rate

Sample	Nuclide	St			Lm			LSDn		
		Age (yr)	Internal error	External error (yr)	Age (yr)	Internal error (yr)	External error (yr)	Age (yr)	Internal error	External error
Ward Creek Fan:										
S1-Lower (Qdfy)										
WCF-Qdfy-S1-lower-1	Be-10 (qtz)	25659	523	2190	24641	501	1999	24796	504	1613
WCF-Qdfy-S1-lower-2	Be-10 (qtz)	16784	347	1411	16421	339	1314	16618	343	1068
WCF-Qdfy-S1-lower-3	Be-10 (qtz)	57035	919	5102	54543	875	4618	54875	881	3697
WCF-Qdfy-S1-lower-4	Be-10 (qtz)	21993	413	1857	21271	399	1707	21443	403	1377
WCF-Qdfy-S1-lower-5	Be-10 (qtz)	23155	432	1958	22331	416	1795	22497	419	1446
WCF-Qdfy-S1-lower-6	Be-10 (qtz)	17604	368	1484	17196	359	1379	17385	363	1120
Ward Creek Fan:										
S1-Upper (Qdfy)										
WCF-Qdfy-S1-upper-1	Be-10 (qtz)	17521	364	1476	17119	355	1372	17301	359	1114
WCF-Qdfy-S1-upper-2	Be-10 (qtz)	18360	380	1548	17904	371	1437	18076	374	1165
WCF-Qdfy-S1-upper-3	Be-10 (qtz)	16661	407	1417	16307	398	1322	16474	402	1080
WCF-Qdfy-S1-upper-4	Be-10 (qtz)	16688	348	1404	16332	340	1308	16495	343	1061
WCF-Qdfy-S1-upper-5	Be-10 (qtz)	13305	273	1112	13086	269	1041	13264	273	847
Ward Creek Fan:										
S2-Lower (Qdfm)										
WCF-Qdfm-S2-lower-1	Be-10 (qtz)	121632	2371	12375	113691	2182	10830	113768	2184	8633
WCF-Qdfm-S2-lower-2	Be-10 (qtz)	122165	2394	12444	114198	2202	10891	114433	2208	8697
WCF-Qdfm-S2-lower-3	Be-10 (qtz)	85411	1516	8083	81004	1425	7230	81487	1435	5795
WCF-Qdfo-S2-lower-4	Be-10 (qtz)	72864	1183	6715	69205	1116	6022	69549	1122	4814
WCF-Qdfm-S2-lower-5	Be-10 (qtz)	133867	2444	13915	124580	2233	12087	124693	2235	9619
Ward Creek Fan:										
S2-Upper (Qdfm)										
WCF-Qdfm-S2-upper-1	Be-10 (qtz)	64751	1030	5873	61754	976	5296	61983	980	4227
WCF-Qdfm-S2-upper-2	Be-10 (qtz)	79410	1719	7496	75356	1619	6719	75441	1621	5386
WCF-Qdfm-S2-upper-3	Be-10 (qtz)	21445	413	1811	20768	399	1668	20892	402	1343
WCF-Qdfm-S2-upper-4	Be-10 (qtz)	66991	1280	6143	63762	1211	5530	63874	1213	4422
WCF-Qdfm-S2-upper-5	Be-10 (qtz)	120130	2335	12185	112331	2150	10672	112296	2149	8496
Lake Como Morraine:										
MC1 (Qgty)										
LCS-Qgty-MC1-upper-1	Be-10 (qtz)	15629	334	1314	15325	327	1227	15504	331	998
LCS-Qgty-MC1-upper-2	Be-10 (qtz)	14356	296	1202	14131	291	1126	14323	295	917
LCS-Qgty-MC1-lower-3	Be-10 (qtz)	16322	345	1373	15982	337	1280	16185	342	1042
LCS-Qgty-MC1-lower-4	Be-10 (qtz)	15911	329	1336	15591	322	1246	15789	326	1013
LCS-Qgty-MC1-fault-5	Be-10 (qtz)	15338	316	1286	15054	310	1202	15236	314	977
Lake Como Morraine:										
MC2 (Qgty)										
LCS-Qgty-MC2-lower-1	Be-10 (qtz)	16676	384	1412	16318	375	1316	16486	379	1072
LCS-Qgty-MC2-lower-2	Be-10 (qtz)	14103	291	1180	13882	287	1106	14069	291	900
LCS-Qgty-MC2-lower-3	Be-10 (qtz)	16481	329	1382	16137	322	1288	16301	326	1044
LCS-Qgty-MC2-upper-4	Be-10 (qtz)	16855	354	1419	16484	346	1321	16646	349	1072
LCS-Qgty-MC2-upper-5	Be-10 (qtz)	21797	464	1852	21084	448	1705	21212	451	1378
LCS-Qgty-MC2-upper-6	Be-10 (qtz)	18435	344	1546	17970	335	1433	18116	337	1156

St: Time-independent scaling age model by Stone et al. (2000), which is based on Lal (1991).
Lm: Time-dependent scaling age model by Lal/Stone that accounts for geomagnetic field variations.
LSDn: Nuclide-dependent scaling age model by Lifton-Stato-Dunai.

Age results generated by CRONUS-Earth online calculators, Blaco et al. (2008).
https://hess.ess.washington.edu/
version 3

Appendix. Detailed descriptions of geological map units in Plate 1.

Qal—Stream alluvium (Holocene and Late Pleistocene)-Subangular to rounded, moderately to well sorted and stratified, pebble to boulder sandy gravel. Gravel clasts representative of drainage basins. Includes flood plain areas of sand, silt, and clay. primarily quartzite, siltite, and volcanic rocks. Includes minor colluvium, fan deposits, and pebbly to cobbly sandy silt in local lower energy drainages. Deposits are 1-18 m (3-60 ft) thick, and average 12 m (40 ft) (McMurtrey and others, 1972).

Qaf—Small alluvial fan and debris-flow deposits (Holocene and Late Pleistocene)-Sub-angular to rounded, poorly sorted, matrix-supported pebble to boulder gravel in a sand, silt, and clay matrix. Commonly grades into, interfingers with, and caps stream alluvium (Qal). Thickness varies greatly, ranging from 1 to 24 m.

Qafo—Older alluvial fan and debris flow deposits (Pleistocene)-Sub-angular to rounded, moderately to poorly sorted pebble to boulder graved in a sand, silt, and clay matrix. Clasts locally derived. Thickness less than 20 meters.

Qpa--Paludal deposit (Holocene)-Sand, silt, clay, and organic matter deposited in swamp, marsh, pond, or lake. Thickness probably less than 10 m (33 ft).

Qatd—Alluvium of the Darby Terrace (late Pleistocene?)-Well-rounded, well-sorted gravel and sand underlying the youngest terrace, underlying most of the town of Darby. The surfaces of these deposits stand 5 to 10 feet above the present floodplain. Thickness estimated at 10 to 20 feet. Predominantly granitic, gneissic, and Belt sedimentary clasts, with minor volcanic clasts.

Qatr—Alluvium of the Riverside Terrace (late Pleistocene?)-Well-rounded, well-sorted gravel and sand underlying the youngest terrace, termed the Riverside terrace by Weber (1972), along the Bitterroot River. The surfaces of these deposits stand 10 to 15 feet above the present floodplain. Thickness estimated at 10 to 20 feet. Predominantly granitic, gneissic, and Belt sedimentary clasts, with minor volcanic clasts.

Qath—Alluvium of the Hamilton Terrace (late Pleistocene?)-Well-rounded, well-sorted gravel and sand underlying the second youngest terrace, the Hamilton terrace (Weber, 1972), along the Bitterroot River. The surfaces of these deposits stand 20 to 25 feet above the present floodplain. Thickness is from 10 to 30 feet. Predominantly granitic, gneissic, and Belt sedimentary clasts, with minor volcanic clasts.

Qgoy—Younger glacial outwash deposits (latest Pleistocene to early Holocene)-Subrounded to well-rounded, moderately sorted, unweathered cobbles and boulders in a matrix of sand and gravel deposited in outwash fans downstream from Pinedale-age glaciers. Surfaces of these deposits are at a lower level than older outwash (Qgoo and Qgom). Can be traced upstream to glacial till deposits of Pinedale age (Qgty). Surfaces of these deposits stand 5-25 feet above the active channels. Some fans appear to coalesce with alluvial terrace deposits (Qatr and Qath). Thickness averages 12 m (McMurtrey and others, 1972).

Qdfy—Younger glacial debris flow deposits (latest Pleistocene to early Holocene)-Subangular to well-rounded, poorly sorted, matrix-supported, unweathered boulders and cobbles in a matrix of sand, gravel, and clay. Characterized by boulders as much as 3 m in diameter, and by a hummocky appearance on the Lidar image. Deposited in debris-flow fans below Pinedale-age glaciers, probably as a result of

catastrophic glacial outburst floods. Good exposures occur on the Ward Creek fan, where the upstream ends overlie the pediment surface, and the downstream ends are incised into the pediment. Thickness probably 2-12 m.

Qgom—Middle-aged glacial outwash deposits (Pleistocene)-Subrounded to well-rounded, moderately sorted, unweathered cobbles and boulders in a matrix of sand and gravel deposited in outwash fans downstream from Pleistocene glaciers. Surfaces of these deposits stand at an intermediate level between younger and older glacial outwash (Qgoy and Qgoo), but their absolute ages are unknown. They can be traced upstream to older glacial till deposits (Qgto). Thickness probably 6-12 m.

Qdfm—Middle-aged glacial debris flow deposits (late Pleistocene)-Subangular to well-rounded, poorly sorted, matrix-supported, unweathered boulders and cobbles in a matrix of sand, gravel, and clay. Characterized by boulders as much as 3 m in diameter, and by a hummocky appearance on the Lidar image. Surfaces of these deposits stand at an intermediate level between younger and older glacial outwash (Qgoy and Qgoo), but their absolute ages are unknown. Deposited in debris-flow fans, probably as a result of catastrophic glacial outburst floods. Thickness probably 2-12 m.

Qgoo—Older glacial outwash deposits (Pleistocene)-Subrounded to well-rounded, moderately sorted, variably weathered cobbles and boulders in a matrix of sand and gravel deposited in outwash fans downstream from Pleistocene glaciers. Surfaces of these deposits lie above the younger outwash fans (Qgoy and Qgom), and they typically mantle pediments developed on the ancestral Bitterroot River deposits (QTgc). Mapped as Tertiary Sixmile Creek Formation on Lonn and Sears (2000) but reassigned to a Pleistocene age herein because they can be traced upstream to older glacial moraines (Ogto). Thickness from 2-12 m.

Qdfo—Older glacial debris flow deposits (Pleistocene)-Subangular to well-rounded, poorly sorted, matrix-supported, variably weathered boulders and cobbles in a matrix of sand, gravel, and clay. Characterized by boulders as much as 3 m in diameter, and by a slightly hummocky appearance on the Lidar image. Deposited in debris-flow fans below Pleistocene glaciers, probably as a result of catastrophic glacial outburst floods. Underlies part of the Ward Creek pediment surface but may also mantle pediments developed on the ancestral Bitterroot River deposits (QTgc). Many were mapped as Tertiary Sixmile Creek Formation on Lonn and Sears (2000) but reassigned to a Pleistocene age herein because they can be traced upstream to older glacial moraines (Ogto). Thickness ranges from 12 m at the heads of fans to less than 2 m near the toes.

Qgty—Younger glacial till deposits (late Pleistocene)-Unsorted, mostly unstratified, clay, silt, sand, and gravel containing boulders up to 6 m in diameter. Clasts subangular to subrounded and unweathered. Deposited in Pinedale-age glacial moraines typically inset within older moraines (Qgto). Characterized by very hummocky appearance on the Lidar image. Thickness probably ranges from 10-120m.

Qgtm—Middle-aged glacial till deposits (Pleistocene)-Unsorted, mostly unstratified, clay, silt, sand, and gravel containing boulders up to 6 m in diameter. Clasts subangular to subrounded and variably weathered. Deposited in Pleistocene glacial moraines. Characterized by their smooth surfaces on the Lidar image in contrast to younger till (Qgty) with well-preserved hummocky topography. Distinguished where middle-aged till can be distinguished; in other areas, it is included in Qgto. Thickness ranges from 10-120 m.

Qgto—Older glacial till deposits (Pleistocene)—Unsorted, mostly unstratified, clay, silt, sand, and gravel containing boulders up to 6 m in diameter. Clasts subangular to subrounded and variably weathered. Deposited in Pleistocene glacial moraines. Characterized by their smooth surfaces on the Lidar image in contrast to younger till (Qgty) with well-preserved hummocky topography. Thickness ranges from 10-120 m.

Qgto/Qgoy—Older glacial till deposits and younger glacial outwash deposits, undivided (Pleistocene)—Mapped where older glacial till underlying the Hayes Creek pediment surface was eroded by meltwater from the Hayes Creek glacier that also deposited younger bouldery outwash gravels. Characterized by a gently undulating surface containing scattered, enormous, angular gneissic and granitic boulders that are badly weathered, and abundant, fresher, well-rounded cobbles and boulders.

QTgc—Gravel and clay of the ancestral Bitterroot River deposits (Oligocene to Plio-Pleistocene?)—Unconsolidated, well-sorted, stratified, well-rounded, fluvial gravel and sand interbedded with light tan clay, silt, and tephra. Deposited in channels and floodplains of the ancestral Bitterroot River (Lonn and Sears, 2000) and tributary streams and fans. Gravel deposits contain well-rounded cobbles and pebbles of (in order of decreasing abundance) Belt quartzite, granite/granodiorite, mylonitic gneiss, high-grade metamorphic rocks, and extrusive volcanic rocks that represent rocks exposed in the entire Bitterroot River drainage. Interbedded finer grained deposits, probably deposited in adjacent floodplains, are light gray clay and silt deposits in beds 6 inches to 5 feet thick, with abundant interbedded tephra. Some brown, ledge-forming massive silty layers with root casts and burrows are present and interpreted to be paleosols. Westward and stratigraphically upward, gravel becomes dominated by granitic and mylonitic gneiss clasts; these are generally well-rounded near the valley center, and are well-rounded to sub-angular, and sometimes bouldery, near the western valley's western edge. Similar in origin and facies relationships to QTgcd (see below). It is unclear whether these upper granitic gravels are Quaternary or Tertiary in age. Fossil assemblages collected by Konizeski (1958; McMurtrey and others, 1972) in the fine-grained intervals ranged from Oligocene to late Miocene in age, and a recently unearthed fossil was estimated to be 7-9 Ma (Dale Hanson, Museum of the Rockies, written communication, 2018). Deep drill holes show that unconsolidated sedimentary rocks similar to QTgc are up to 700 meters thick in places (Norbeck, 1980). Unit QTgc also occurs 450 m above the valley floor along the Bitterroot Mountain front in the northern Bitterroot map area where it is interpreted to have been elevated to this position by faults. Lower contact is exposed in two places on the southern Bitterroot map where QTgc unconformably overlies brecciated granitic bedrock. Upper contact is an erosional (pediment) surface; the occurrence of Pleistocene glacial deposits under some pediments suggests a Pleistocene age.

Tv—Volcanic rocks (Eocene?)-Rhyolite tuff and andesite flows. Age unknown but thought to be Eocene and related to extension associated with the B-detachment fault (Berg and Lonn, 1996).

TKg—Foliated granodiorite and unfoliated granite with mylonitic zones, undivided (Cretaceous and Eocene)-In the footwall of the Bitterroot detachment, unit is weakly foliated to gneissic (mylonitic) Cretaceous to Eocene biotite-muscovite granodiorite intruded by unfoliated Eocene biotite-muscovite granite. Fabrics and mylonitization in the granodiorite developed at deep levels early in Bitterroot detachment fault's history, while the Eocene granite intruded at shallow levels following most of the plastic deformation. In the B-detachment hanging wall, both unfoliated Eocene biotite-muscovite granite and foliated to unfoliated biotite-muscovite granodiorite occur. Unit also includes outcrop-scale inclusions

of Belt metasedimentary rock that are too small to show on the map. A thick brecciated zone occurs along the B-detachment fault and is marked by breccia symbols on the maps.

YXm—Metamorphic rocks (Paleoproterozoic)-Quartzite, amphibolite, and calc-silicate gneiss continuous with the postulated basement rocks of Sleeping Child Creek in the Sapphire Mountains in the hanging wall of the Bitterroot detachment. A U-Pb crystallization age of 1860 Ma was obtained for the Sleeping Child orthogneiss while detrital zircons from two quartzite samples suggest a Belt Supergroup protolith with a maximum age of about 1378 Ma (Lonn and Mosolf, 2020).